The Impact of Monthly Variation of the Pacific-North America (PNA) Teleconnection Pattern on Wintertime Surface-layer Aerosol Concentrations in the United States

Jin Feng[1,2], Hong Liao[3,*], Jianping Li[4]

[1]State key Laboratory of Atmospheric Boundary Layer Physics and Atmospheric Chemistry, Institute of Atmospheric Physics, Chinese Academy of Sciences, Beijing, China

[2]University of Chinese Academy of Science, Beijing, China

[3]School of Environmental Science and Engineering, Nanjing University of Information Science & Technology, Nanjing, China

[4]College of Global Change and Earth System Science of Beijing Normal University, Beijing, China

*Corresponding author address:

Prof. Hong Liao

School of Environmental Science and Engineering

Nanjing University of Information Science & Technology

Nanjing 210044, China

E-mail: hongliao@nuist.edu.cn

Abstract

The Pacific-North America teleconnection (PNA) is the leading general circulation pattern in the troposphere over the region of North Pacific to North America during wintertime. This study examined the impacts of monthly variation of the PNA phase (positive or negative phase) on wintertime surface-layer aerosol concentrations in the U.S. by analyzing observations during 1999–2013 from the Air Quality System of the Environmental Protection Agency (EPA-AQS) and the model results for 1986–2006 from the global three-dimensional Goddard Earth Observing System (GEOS) chemical transport model (GEOS-Chem). The composite analyses on the EPA-AQS observations over 1999–2013 showed that the average concentrations of $PM_{2.5}$, sulfate, nitrate, ammonium, organic carbon, and black carbon aerosols over the U.S. were higher in the PNA positive phases (25% of the winter months examined, and this fraction of months had the highest positive PNA index values) than in the PNA negative phases (25% of the winter months examined, and this fraction of months had the highest negative PNA index values) by 1.0 μg m^{-3} (8.7%), 0.01 μg m^{-3} (0.5%), 0.3 μg m^{-3} (29.1%), 0.1 μg m^{-3} (11.9%), 0.6 μg m^{-3} (13.5%), and 0.2 μg m^{-3} (27.8%), respectively. The simulated geographical patterns of the differences in concentrations of all aerosol species between the PNA positive and negative phases were similar to observations. Based on the GEOS-Chem simulation, the pattern correlation coefficients were calculated to show the impacts of PNA-induced variations in meteorological fields on aerosol concentrations. The PNA phase was found to influence sulfate concentrations mainly through changes in planetary boundary layer height (PBLH), precipitation (PR), and temperature, to influence nitrate concentrations mainly through changes in temperature, and to influence concentrations of ammonium, organic carbon, and black carbon mainly through

51 changes in PR and PBLH. Results from this work have important implications for
52 understanding and prediction of air quality in the United States.

1 Introduction

Aerosols are the major air pollutants that have adverse effects on human health, reduce atmospheric visibility, and influence climate through aerosol-radiation and aerosol-cloud interactions (IPCC, 2013). Aerosol concentrations are high over the industrialized regions such as the U.S., Europe, and East Asia, which are driven by emissions of aerosols and aerosol precursors (Dutkiewicz et al. 2000; Vestreng et al. 2007; Hand et al. 2012a; Mijling et al. 2013) and regional meteorological conditions.

Previous studies have shown that aerosol concentrations are very sensitive to meteorological parameters (Aw and Kleeman 2003; Wise and Comrie 2005; Dawson et al. 2007; Kleeman 2008; Jacob and Winner 2009; Tai et al. 2010; Tai et al. 2012a; Allen et al. 2015; Markakis et al. 2015; Megaritis et al. 2014; Porter et al. 2015). Aw and Kleeman (2003) examined the sensitivity of $PM_{2.5}$ (aerosol particles which diameter ≤ 2.5 μm) concentration to temperature by performing sensitivity studies in the California Institute of Technology/UC Davis (CIT/UCD) air quality model. A cross-board increase in temperature by 5 K in Southern California on September 25, 1996, led to decreases in peak $PM_{2.5}$ concentrations by up to 30.7 μg m^{-3} (~30%). Wise and Comrie (2005) reported, by statistical analyses of observational datasets obtained from Air Quality System of U.S. Environmental Protection Agency (EPA-AQS), that the variations in meteorological parameters accounted for 20–50% of the variability in aerosol levels over 1990–2003 in five metropolitan areas in the southwestern U.S.. They found that aerosols in these five cities were most sensitive to relative humidity. Dawson et al. (2007) found, by sensitivity studies in the Particulate Matter Comprehensive Air Quality Model with extensions (PMCAMx), that $PM_{2.5}$ concentrations in summer had a small sensitivity to temperature increases (−16 ng m^{-3} K^{-1} on average) because the increases in sulfate offset the decreases in

78 nitrate and organics, while $PM_{2.5}$ concentrations in winter decreased significantly with
79 temperature (−170 ng m^{-3} K^{-1} on average) because the increases in temperature led
80 to large reductions in nitrate and organics. Dawson et al. (2007) also showed that
81 $PM_{2.5}$ concentrations increased with humidity in both winter and summer. Jacob and
82 Winner (2009) summarized by literature review that the regional stagnation, mixing
83 depth, and precipitation are the most important meteorological parameters that
84 influence surface-layer aerosol concentrations. Future climate change was also
85 simulated to influence aerosol levels over the U.S. by –1 to +1 μg m^{-3} (Jacob and
86 Winner 2009), as a result of the climate-induced changes in atmospheric oxidants,
87 transport, deposition, and the shift of gas-particle equilibria (Liao et al. 2006; Unger et
88 al. 2006; Bauer et al. 2007; Jacob and Winner 2009; Pye et al. 2009; Lam et al. 2011;
89 Day and Pandis 2011; Juda-Rezler et al. 2012; Tai et al. 2012b).
90 Previous studies have also reported that the changes in atmospheric circulation
91 pattern and climate systems, such as the East Asian Summer Monsoon (EASM),
92 North Atlantic Oscillation (NAO), El Nino-South Oscillation (ENSO), Atlantic
93 Multidecadal Oscillation (AMO), and Arctic sea ice (ASI), can modulate distributions
94 and concentrations of aerosols (Moulin et al. 1997; Singh and Palazoglu 2012; Zhu et
95 al. 2012; Jerez et al. 2013; Liu et al. 2013; Xiao et al. 2014; Wang et al. 2015). Zhu et
96 al. (2012) found, by simulation of aerosol concentrations over years 1986–2006 with
97 the global chemical transport model GEOS-Chem, that the decadal-scale weakening
98 of the EASM led to increases in aerosol concentrations in eastern China, and
99 summertime surface aerosol concentrations in the weakest EASM years were larger
100 than those in the strongest EASM years by approximately 20%. Moulin et al. (1997)
101 showed that the variations in NAO could influence mineral dust aerosol transported to
102 the North Atlantic Ocean and the Mediterranean Sea, since the mean aerosol optical

depth (AOD) of dust in summer correlated with the NAO index during 1983–1994 with the correlation coefficients of 0.49 and 0.66 respectively. Jerez et al. (2013) found, by simulations of aerosols for years 1970–1999 with the CHIMERE chemistry transport model driven by the BCMWF ERA40 reanalysis data, that the concentrations of PM_{10} and $PM_{2.5}$ in European differed by 10 and 20 μg m^{-3}, respectively, between the positive and negative NAO phases. By using the multi-angle imaging spectroradiometer satellite (MISR) datasets of AOD during 2000–2011, Liu et al. (2013) found a period of 3–4 years in observed summertime AOD over the North China Plain (NCP), and the peak of summertime AOD in NCP occurred four months later after the rapidly transition of El Nino from a warm phase to a cold phase because of the associated cyclone anomaly and maritime inflow over the NCP. Singh and Palazoglu (2012) found correlations between PDO and ENSO and the aerosol exceedance days (defined as the days with $PM_{2.5}$ concentrations larger than the U.S. National Ambient Air Quality Standard) at 6 regions in the U.S. by using the EPA-AQS $PM_{2.5}$ wintertime datasets during 1950–2008.

The Pacific-North America teleconnection pattern (PNA) is one of the most recognized, influential climate patterns in the mid-latitudes over the region of North Pacific to North America during wintertime with monthly variations (Wallace and Gutzler 1981; Blackmon et al. 1984; Liang et al. 2005; Athanasiadis and Ambaum 2009). The PNA phase is defined by the geopotential height anomalies in the middle troposphere over the vicinity of Hawaii, the south of the Aleutian Islands, the intermountain region of North America, and the Gulf Coast region in the U.S. (Wallace and Gutzler 1981). A positive (negative) PNA phase is characterized by positive (negative) geopotential height anomalies over the vicinity of Hawaii and the northwestern North America, while negative (positive) geopotential height anomalies

over south of the Aleutian Islands and the Gulf Coast region (see Fig. S1 in the auxiliary material).

The PNA has large impacts on surface-layer meteorological variables in the U.S. during wintertime. Previous studies have reported strong positive (negative) correlation between PNA and surface ambient temperature in the northwestern (southeastern) U.S. (Leathers et al. 1991; Redmond and Koch 1991; Liu et al. 2015), and negative correlation between PNA and precipitation rate (Leathers et al. 1991; Coleman and Rogers 2003; Ning and Bradley 2014; 2015) and moisture (Coleman and Rogers 2003) in the contiguous Ohio River Valley. These variations in meteorological parameters in the U.S. are associated with the PNA-induced anomalies in jet stream position, activities of cold fronts, and synoptic cyclones (Leathers et al. 1991; Notaro et al. 2006; Myoung and Deng 2009).

Several studies have examined the impacts of PNA on aerosols. Gong et al. (2006) studied the interannual variations in the trans-Pacific transport of Asian dust during 1960–2003 by using the Northern Aerosol Regional Climate Model (NARCM). They found a negative correlation (with a correlation coefficient of –0.55) between the PNA and the ratio of dust mass that reached the North American continent to that exported from Asia because of the strong westerly jet in the East Pacific during the negative PNA phases. Di Pierro et al. (2011), by using satellite retrieval of aerosol optical depth (AOD) from Cloud-Aerosol Lidar with Orthogonal Polarization (CALIOP), identified 11 events of Asian aerosol transport to the Arctic during 2007 to 2009, in which 4 events were associated with the negative PNA phases. These studies, however, were focused on the impact of PNA on the transport of aerosols due to the variations in westerly jet stream and blocking activity. Furthermore, these studies were limited to aerosols in the regions of North America and the Arctic.

We examine in this work the impacts of monthly variations in PNA phase on aerosol concentrations in the U.S. during wintertime, by analyses of the observed aerosol concentrations during 1999–2013 from EPA-AQS and also by simulations of aerosol concentrations for years 1986–2006 using the global chemical transport model GEOS-Chem. The scientific goals of this work are (1) to quantify the differences in wintertime concentrations of sulfate (SO_4^{2-}), nitrate (NO_3^-), ammonium (NH_4^+), black carbon (BC), organic carbon (OC), and $PM_{2.5}$ in the U.S. between different PNA phases, and (2) to understand the roles of PNA-induced variations in meteorology (for example, surface air temperature, wind speed, planetary boundary layer height, precipitation, and relative humidity) in influencing the wintertime aerosol concentrations. The definition of the PNA index, the EPA-AQS observation data used in this work, and the numerical simulation with the GEOS-Chem model are described in Sect. 2. Sections 3 and 4 present the impacts of the PNA on wintertime aerosol concentrations in the U.S. obtained from the EPA-AQS observations and the GEOS-Chem simulation, respectively. The mechanisms for the impacts of PNA on aerosols are examined in Sect. 5.

2 Data, simulation, and methodology

2.1 Observed aerosol concentrations

Observed concentrations of aerosols are obtained from the Air Quality System of the U.S. Environmental Protection Agency (EPA-AQS, http://www.epa.gov/airquality/airdata/). The EPA-AQS daily $PM_{2.5}$ mass concentrations are available over 1999–2013 at about 1200 sites, and the speciated aerosol concentrations, including those of SO_4^{2-}, NO_3^-, NH_4^+, BC and OC, are available for 2000–2013 at about 300 sites.

178 The measurements of aerosol concentrations from the EPA-AQS were carried
179 out at various time intervals (for example, with measurements every one, three or six
180 days) at different sites, and there were plenty of missing values at many sites. The
181 observed concentrations are pre-processed following the three steps: (1) For a
182 specific site, the observations are used in our analyses if the site had at least 5
183 months of observations and there were at least 5 observation records within each
184 month. (2) The mean seasonal cycle in aerosol concentrations in the months of
185 November-March is removed (the aerosol concentrations without seasonal cycle are
186 defined as $C'_{i,j} = C_{i,j} - \frac{1}{n}\sum_{i=1}^{n} C_{i,j}$, where $C_{i,j}$ is the aerosol concentrations in month *j*
187 of year *i, n* is the number of years examined). Such deseasonality approach was used
188 in previous studies that examined the monthly variations in mineral dust aerosol
189 (Cakmur et al. 2001; Mahowald et al. 2003), the decreasing trends in observed $PM_{2.5}$
190 concentrations and satellite AOD in the southeastern U.S. over 2000–2009 (Alston et
191 al. 2012), and the monthly variations in global AOD (Li et al. 2013). (3) Since the
192 observed aerosol concentrations exhibited a significant decreasing trend from 1999
193 to present in the U.S. due to the reductions in emissions of aerosols and aerosol
194 precursors (Alston et al. 2012,
195 http://www3.epa.gov/airtrends/aqtrends.html#comparison), the long-term linear trend
196 in concentrations is identified by the least-square fit and then removed from the
197 wintertime observed concentrations for each site. The EPA-AQS sites with
198 measurements that meet the criteria described in (1) are shown in Fig. 1.

199 **2.2 GEOS-Chem Simulation**

200 We also examine the impacts of PNA on simulated aerosol concentrations in the U.S.
201 by using the GEOS-Chem model (version 8-2-1, http://acmg.seas.harvard.edu/geos).
202 The GEOS-Chem model is a global chemical transport model driven by the

assimilated meteorological fields from the Goddard Earth Observing System (GEOS) of the NASA Global Modeling and Assimilation Office (GMAO). The version of the model we use has a horizontal resolution of 2° ×2.5° and 30 hybrid sigma-P layers from the surface to 0.01 hPa altitude. The model has a fully coupled simulation of tropospheric O_3-NO_x-VOC chemistry and aerosols including SO_4^{2-}, NO_3^-, NH_4^+, BC, OC (Park et al. 2003; Park et al. 2004), mineral dust (Fairlie et al. 2007), and sea salt (Alexander et al. 2005). Considering the large uncertainties in chemistry schemes of secondary organic aerosol (SOA), SOA in our simulation is assumed to be the 10% carbon yield of OC from biogenic terpenes (Park et al., 2003) and 2% carbon yield of OC from biogenic isoprene (van Donkelaar et al., 2007; Mu and Liao, 2014). We mainly examine simulated anthropogenic aerosols from the GEOS-Chem simulation, since mineral dust concentrations in winter are very small (Malm et al. 2004; Zhang et al. 2013) and sea salt is not a major aerosol species in the U.S. (Malm et al. 2004).

The model uses the advection scheme of Lin and Rood (1996), the deep convective scheme of Zhang and McFarlane (1995), the shallow convection scheme of Hack (1994), the wet deposition scheme of Liu et al. (2001), and the dry deposition scheme of Wesely (1989) and Wang et al. (1998). The instantaneous vertical mixing in the planetary boundary layer (PBL) is accounted for by the TURBDAY mixing scheme (Bey et al., 2001). The average PBL height in wintertime in the U. S. is about 480 m and occupies the lowest 3–6 vertical model layers.

We simulate aerosols for years of 1986–2006 driven by the GEOS-4 reanalysis data. The years of 1986–2006 are chosen for chemistry-aerosol simulation because these are the years that the GEOS-4 datasets are available. Global anthropogenic emissions are from the Global Emissions Inventory Activity (GEIA) (Park et al. 2004; Park et al. 2006; Zhu et al. 2012; Yang et al. 2015). Anthropogenic emissions over the

U.S. are overwritten by the U.S. EPA National Emission Inventory for 1999 (NEI99), which have monthly variations in emissions of precursors including SO_2, NO_x, and NH_3. Monthly biomass burning emissions are taken from the Global Fire Emissions Database version 2 (GFED-2) (Giglio et al. 2006; van der Werf et al. 2006). During the simulation of aerosols for years of 1986–2006, the global anthropogenic and biomass burning emissions of aerosols and aerosol precursors are fixed at year 2005 levels, so that the variations in aerosol concentrations are caused by variations in meteorological parameters alone.

Natural emissions of O_3 precursors, including biogenic NMVOCs and NO_x from lighting and soil, are allowed to vary over 1986–2006 following the variations in the GEOS-4 meteorological parameters. Biogenic NMVOC emissions are calculated using the module of Model of Emissions of Gases and Aerosols from Nature (Guenther et al. 2006). Lightning NO_x emissions are described by Sauvage et al. (2007) and Murray et al. (2012). Soil NO_x emissions are calculated using the algorithm proposed by Yienger and Levy (1995).

The GEOS-Chem simulation of aerosols in the U.S. have been evaluated extensively by previous studies (Park et al. 2003; Park et al. 2004; Park et al. 2005; Heald et al. 2006; van Donkelaar et al. 2006; Liao et al. 2007; Heald et al. 2008; van Donkelaar et al. 2008; Fu et al. 2009; Drury et al. 2010; Leibensperger et al. 2011; Zhang et al. 2012). These studies have shown that the GEOS-Chem model can capture the magnitudes and distributions of aerosols in the U.S.. The OH concentrations in GEOS-Chem were examined by previous studies (Holmes et al., 2013; Wu et al., 2007) by calculating the methane lifetime, which agreed closely with the lifetime of 11.2±1.3 yr constrained by methyl chloroform observations by Prather et al. (2012). Previous studies also showed that aerosol concentrations were not so

253 sensitive to OH concentrations in the GEOS-Chem simulations (Heald et al., 2012).

254

255 **2.3 PNA index**

256 The PNA index (PNAI) is commonly used to quantify the changes in PNA phase
257 (Wallace and Gutzler 1981; Leathers et al. 1991). This study follows the definition of
258 PNAI by Leathers et al. (1991). In order to examine the monthly variations in PNA, the
259 mean seasonal cycle of geopotential height at 700 hPa is removed for the months of
260 November, December, January, February, and March (NDJFM) in the studied years.
261 Such deseasonality approach has been used in the analyses of the growth and decay
262 of PNA phase in NDJFM (Feldstein 2002), the development of NAO (Feldstein 2003),
263 the influence of NAO on precipitation in Europe (Qian et al. 2000), and the variations
264 in Madden–Julian oscillation (Wheeler and Hendon 2004). If we are concerned with
265 the PNAI during *n* years, the monthly PNAI in month *j* (*j* is one of the 5 months of
266 NDJFM) of year *i* is calculated by:

267 $$PNAI = \frac{1}{3}\left[-Z^{*\prime}_{i,j}(47.9°N, 170°W) + Z^{*\prime}_{i,j}(47.9°N, 110°W) - Z^{*\prime}_{i,j}(29.7°N, 86.3°W)\right] \quad (1)$$

268 where $Z^{*\prime}_{i,j} = \frac{Z'_{i,j}}{\sqrt{\frac{1}{n\times 5}\sum_{i=1}^{n}\sum_{j=1}^{5} {Z'_{i,j}}^2}}$ and $Z'_{i,j} = Z_{i,j} - \frac{1}{n}\sum_{i=1}^{n} Z_{i,j}$. Therefore, $Z'_{i,j}$ denotes the

269 removal of seasonal cycle, and $Z^{*\prime}_{i,j}$ denotes the standardized anomaly of
270 geopotential height at 700 hPa in month *j* of year *i* with seasonal-cycle removed.

271 The PNAI is calculated by using both the National Center of Environmental
272 Prediction-Department of Energy Atmospheric Model Inter-comparison Project
273 Reanalysis data (NCEP-2, horizontal resolution 2.5°×2.5° globally,
274 http://www.esrl.noaa.gov/psd/data/gridded/data.ncep.reanalysis2.html) for years of
275 1986–2013 (referred to as NCEP2-PNAI) and the GEOS-4 assimilated
276 meteorological data (referred to as GEOS4-PNAI) for 1986–2006 (Fig. 2). Both series

277 of PNA index show strong monthly variations (Fig. 2), and the GEOS4-PNAI agrees
278 with NCEP2-PNAI over 1986–2006 with a high correlation coefficient of 0.99,
279 indicating that the NCEP-2 and GEOS-4 datasets are consistent in representing the
280 monthly variations of PNAI.

281 There are n·5 PNAI values for *n* years, since we calculate PNAI for the months of
282 NDJFM of each year. These *n*·5 PNAI values are classified into 3 categories for our
283 composite analyses of aerosol concentrations and meteorological parameters: the
284 positive PNA months (PNA+) that are 25% of the *n*·5 PNAI months with the highest
285 positive PNAI values, the negative PNA months (PNA–) that are 25% of the *n*·5 PNAI
286 months with the highest negative PNAI values, and the rest months that are referred
287 to as the transitional months (Fig. 2).

288

289 **3 Impacts of PNA on observed aerosol concentrations**

290 The measurements of $PM_{2.5}$ are available over 1999–2013, in which there were 18
291 PNA+ months and 18 PNA– months as shown in Fig. 2a. Figure 3 shows the
292 differences in observed surface-layer $PM_{2.5}$ concentrations between the PNA+ and
293 PNA– months (concentrations averaged over the 18 PNA+ months minus those
294 averaged over the 18 PNA– months). The uncertainty associated with the differences
295 in aerosol concentrations between PNA+ and PNA– months is represented by the
296 two-tail Student-t test with significance level of 90%. Among 1044 sites with $PM_{2.5}$
297 concentrations (Fig.1), 42% of which had statistically significant differences in $PM_{2.5}$
298 between PNA+ and PNA– months. Relative to the PNA– months, $PM_{2.5}$
299 concentrations in PNA+ months were higher in California, the contiguous Salt Lake
300 (northern Utah), and over and near the eastern Midwest. The maximum enhancement
301 of $PM_{2.5}$ reached 7–9 μg m^{-3} (or 40–80%) in California, 7–9 μg m^{-3} (80–100%)

around the Salt Lake, 3–5 μg m^{-3} (40–80%) over and near the eastern Midwest. At sites in North Dakota, Wisconsin, Michigan, Minnesota, Montana, Texas and Maine, the $PM_{2.5}$ concentrations were lower by up to 2 μg m^{-3} (–10 to –20%) in PNA+ months than in PNA– months. As the concentrations are averaged over all sites (including the sites that pass and do not pass the t-test with 90% confidence level) in the U.S., the western U.S. (west of 100°W, Fig.1), and the eastern U.S. (east of 100°W, Fig. 1), $PM_{2.5}$ concentrations were higher by 1.0 μg m^{-3} (8.7%), 1.3 μg m^{-3} (14.3%), and 0.8 μg m^{-3} (7.2%), respectively, in the PNA+ months than in PNA– months (Table 1).

The measurements of speciated aerosols are available during 2000–2013, in which there were 17 PNA+ and 17 PNA– months (Fig. 2b). Figure 3 also shows the differences in observed surface-layer concentrations of individual aerosol species between the PNA+ and PNA– months. The differences in concentrations of SO_4^{2-}, NO_3^- and NH_4^+ show statistically significant positive values at most sites. Among the 355, 343, and 194 sites with measurements of SO_4^{2-}, NO_3^- and NH_4^+, 30%, 44%, and 39% of which pass the two-tail t-test with 90% confidence level, respectively. While the absolute differences in concentrations of SO_4^{2-}, NO_3^- and NH_4^+ between PNA+ and PNA– were in the range of 0–1 μg m^{-3} at most sites, the maximum differences reached 1.5–2.5 μg m^{-3} (30–50%) for SO_4^{2-} in Pennsylvania, 1.5–2.5 μg m^{-3} (150–200%) for NO_3^- in Illinois, Indiana and Ohio, and 1.5–2.5 μg m^{-3} (50–70%) for NH_4^+ in Pennsylvania. Averaged over the sites with measurements, the absolute differences in concentrations of SO_4^{2-} and NO_3^- between PNA+ and PNA– months were larger in the eastern U.S. than in the western U.S.. As shown in Table 1, the differences in the averaged concentrations of SO_4^{2-}, NO_3^- and NH_4^+ were, respectively, 0.1 μg m^{-3} (3.7%), 0.4 μg m^{-3} (36.5%), and 0.1 μg m^{-3} (10.5%) in the eastern U.S., 0.03 μg m^{-3}

326 (3.2%), 0.2 μg m^{-3} (23.8%), and 0.2 μg m^{-3} (31.6%) in the western U.S., as well as
327 0.01 μg m^{-3} (0.5%), 0.3 μg m^{-3} (29.1%), and 0.1 μg m^{-3} (11.9%) in the whole of U.S..
328 With regard to carbonaceous aerosols, among the 105 and 104 sites with
329 measurements of OC and BC, 39% and 31% of which pass the two-tail t-test with 90%
330 confidence, respectively. The differences in concentrations of these two species
331 between PNA+ and PNA– months show similar geographical pattern, with positive
332 values at most sites but negative values in Michigan, New York, and the South
333 Atlantic States. The maximum differences between the PNA+ and PNA– months
334 reached 2.5–3 μg m^{-3} (50–70%) in Kentucky for OC. Averaged over sites with
335 measurements available, the absolute differences in OC and BC concentrations
336 between the PNA+ and PNA– months were larger in the western U.S. than in the
337 eastern U.S. (Table 1). Among all aerosol species listed in Table 1, OC exhibited the
338 largest absolute differences between the PNA phases in the western U.S., because
339 OC accounts for 25–65% of $PM_{2.5}$ in the western U.S. (Malm et al. 2004) and the OC
340 observed by EPA-AQS network, which are located in urban and suburban settings,
341 were higher than the observations by other long term networks in U.S..(Malm et al.
342 2011, Rattigan et al. 2011, Hand et al. 2012b, 2014).
343 Observations from EPA-AQS datasets indicate the large impacts of PNA phase
344 on aerosol concentrations in the U.S.. It should be noted that, in our analyses above,
345 the locations of measurements and the numbers of samples were different for
346 different aerosol species. The regional averages were also influenced by the uneven
347 distributions of observational sites in different regions. Therefore, model results from
348 the GEOS-Chem simulation will be used to further analyze the impacts of PNA on
349 aerosols in the U.S., as presented in the subsequent sections.

We have also calculated the correlation coefficient between PNAI and EPA-AQS surface aerosol concentrations at each site for each aerosol species ($PM_{2.5}$, SO_4^{2-}, NO_3^-, NH_4^+, OC, or BC) (see auxiliary Fig. S2). About 40%, 30%, 47%, 33%, 33% and 34% of sites pass the two-tail t-test with 90% confidence for $PM_{2.5}$, SO_4^{2-}, NO_3^-, NH_4^+, OC and BC, respectively. At most sites, positive (negative) correlation coefficients in Fig. S2 corresponded to the increases (decreases) in aerosol concentration in PNA+ months relative to PNA– months shown in Fig. 3. Positive correlation coefficients were large over California, the contiguous Salt Lake, and over and near the eastern Midwest. The fraction of temporal variability explained by PNA (FTVEP) can be quantified approximately by the square of correlation coefficient (http://mathbits.com/MathBits/TISection/Statistics2/correlation.htm) (see auxiliary Fig. S3). For all aerosol species, FTVEP were about 5–15% at most sites. For $PM_{2.5}$, SO_4^{2-}, NO_3^- and NH_4^+ aerosols, FTVEP values were high over and near the eastern Midwest, where the PNA teleconnection explained up to 50%, 40%, 50%, and 40% of temporal variances of surface concentrations of these aerosol species, respectively.

4 Impacts of PNA on simulated aerosol concentrations

4.1 Simulated aerosol concentrations and model evaluation

Fig. 4a shows the simulated surface-layer concentrations of $PM_{2.5}$ (the sum of SO_4^{2-}, NO_3^-, NH_4^+, BC, and OC) and each aerosol species averaged over NDJFM of 1999–2006. These years are selected because they are the common years of model results and EPA-AQS observation datasets. The simulated $PM_{2.5}$ concentrations were higher in the eastern U.S. than in the western U.S.. The maximum surface $PM_{2.5}$ concentrations reached 14–16 μg m^{-3} in Ohio and Pennsylvania. $PM_{2.5}$ concentrations in the western U.S. were generally less than 4 μg m^{-3}, except for

375 California where $PM_{2.5}$ concentrations were 2–6 μg m^{-3}. The distribution of SO_4^{2-} was
376 similar to that of $PM_{2.5}$, with higher concentrations in the eastern U.S. (1–8 μg m^{-3})
377 than in the western U.S. (0–3 μg m^{-3}) due to the coal-fired power plants in the
378 Midwest (Park et al. 2006). The concentrations of NO_3^- and NH_4^+ were the highest
379 over and near the eastern Midwest, with values of 3–4 and 2–3 μg m^{-3}, respectively.
380 The maximum OC concentrations were simulated to be 2–3 μg m^{-3} in two regions,
381 from Ohio to Massachusetts and from Alabama to South Carolina. The simulated BC
382 concentrations in the U.S. were 0–1 μg m^{-3}, except for the contiguous New York
383 where BC concentrations reached 1–2 μg m^{-3}. The magnitudes and geographic
384 distributions of SO_4^{2-}, NO_3^-, NH_4^+ concentrations simulated in our work are similar to
385 those simulated by Park et al. (2006) and Pye et al. (2009), and our simulated OC
386 and BC were similar to those reported by Park et al. (2003).
387 Figure 4b presents the scatter plots of the simulated concentrations versus the
388 EPA-AQS observations. The simulated $PM_{2.5}$ concentrations had normalized mean
389 bias ($NMB = \sum_{m=1}^{M}(S_m - O_m) / \sum_{m=1}^{M}(O_m) \times 100\%$, where S_m and O_m are the
390 simulated and observed aerosol concentrations in month *m*, respectively. *M* is the
391 total number of winter months examined) of –30% over the U.S., and the correlation
392 coefficient between simulated and observed $PM_{2.5}$ concentrations was 0.57. The
393 simulated wintertime SO_4^{2-}, NO_3^- and NH_4^+ had NMBs of 37%, 4%, and 26%,
394 respectively. Similar bias in simulated SO_4^{2-} in December-January-February (DJF)
395 was reported Park et al. (2006), as the GEOS-Chem model results were compared
396 with observations from the Clean Air Status and Trends Network (CASTNET). The
397 high bias in our simulated NH_4^+ was associated with the overestimation of SO_4^{2-}. Our
398 model underestimates $PM_{2.5}$, SO_4^{2-}, NO_3^-, NH_4^+, OC and BC in the western U.S. (Fig.

399 4b), which can be explained in part by the relatively high aerosol concentrations
400 observed for this region from the EPA-AQS. Hand et al. (2014) compared the
401 observed concentrations of aerosols from the EPA-AQS with those from the
402 Interagency Monitoring of Protected Visual Environments (IMPROVE) for 2008–2011,
403 and showed that the ratios of wintertime aerosol concentrations of ammonium sulfate,
404 ammonium nitrate, OC, and BC from the EPA-AQS to those from the IMPROVE were,
405 respectively, 2.3, 7.7, 8.3, and 13.1, as the concentrations were averaged over the
406 western U.S.. Liu et al. (2004) also attributed the high EPA-AQS concentrations in the
407 western U.S. to the relative sparse urban sites that were heavily influenced by strong
408 local sources such as automobiles and wood fires. The low model biases in the
409 western U.S. may also be caused by the biases in emissions in the model.
410 Since this study is dedicated to examine the influence of PNA phase on the
411 month-to-month variations of aerosol concentrations during wintertime, Fig. 4c
412 compares, for each aerosol species, the deviation from the mean (DM) of observed
413 concentration with that of simulated concentration for each winter month. The DM is
414 defined as $DM_m = \left(C_m - \frac{1}{M}\sum_{m=1}^{M} C_m\right) / \frac{1}{M}\sum_{m=1}^{M} C_m$, where C_m is the simulated
415 average aerosol concentration over the U.S. in month *m*, and *M* is the number of
416 winter months examined (we consider the months of NDJFM over 1999–2006 for
417 $PM_{2.5}$, and the months of NDJFM over 2000–2006 for SO_4^{2-}, NO_3^-, NH_4^+, BC, and OC).
418 The model captures fairly well the peaks and troughs of DMs for $PM_{2.5}$, SO_4^{2-}, NO_3^-
419 and NH_4^+, with correlation coefficients of 0.61, 0.45, 0.33, and 0.65, respectively. The
420 model does not capture well the monthly variations of DMs of concentrations of OC
421 and BC, because both anthropogenic and biomass burning emissions are fixed at
422 year 2005 levels during our simulation over 1986–2006 to isolate the impacts of
423 variations in meteorological parameters (PNA phases) on aerosols (see Sect. 2.2).

Since the biomass burning emissions, which contribute largely to carbonaceous aerosols, have large interannual variations (Duncan et al., 2003; Generoso et al., 2003; van der Werf et al., 2006), we also show in Fig. 4c the time series of DMs of biomass burning emissions of OC and BC by using biomass burning emissions in NDJFM over 2000–2006 from GFED v2. The correlation coefficients between biomass burning emissions and observed concentrations of OC and BC were 0.36 and 0.34, respectively, indicating that the observed variations in OC and BC were influenced by monthly and interannual variations in biomass burning. We have also calculated the temporal correlation coefficient between EPA-AQS observations and GEOS-Chem model results at each site for each aerosol species (auxiliary Fig. S4). The temporal correlations were statistically significant for $PM_{2.5}$, SO_4^{2-}, NO_3^-, NH_4^+ at most sites in the U.S., especially over and near the eastern Midwest where largest increases in aerosol concentrations were identified in the PNA+ months relative to the PNA– months.

4.2 Impact of PNA on simulated surface-layer aerosol concentrations

We have performed the GEOS-Chem simulation for years 1986–2006, in which there were 35 PNA+ and 35 PNA– months (Fig. 2). Figure 5a shows the concentrations of $PM_{2.5}$ and each aerosols species (SO_4^{2-}, NO_3^-, NH_4^+, BC, and OC) averaged over the PNA– months of 1986–2006. The magnitudes and geographic distributions of aerosol concentrations in PNA– months were similar to those averaged over NDJFM of years 1999–2006 in Fig. 4.

The simulated absolute and relative differences in aerosol concentrations between PNA+ and PNA– months are shown in Figs. 5b and 5c. The $PM_{2.5}$ concentrations over the U.S. are simulated to increase in PNA+ relative to PNA–

449 months. The maximum enhancement in $PM_{2.5}$ concentrations in PNA+ months was
450 1.8–2.4 μg m^{-3} (20–40%), located in the juncture of Tennessee and Arkansas. Note
451 that the pattern of simulated differences in $PM_{2.5}$ between PNA+ and PNA–months
452 was similar to that of observations (Fig. 3), except that the simulated differences were
453 not large in California, mainly due to the underestimation of OC in California as
454 compared to EPA-AQS data (Fig. 4b). The simulated $PM_{2.5}$ concentrations were
455 higher by 0.6 μg m^{-3} (12.2%), 0.3 μg m^{-3} (14.0%), and 0.9 μg m^{-3} (10.8%) over the
456 whole of, western, and eastern U.S., respectively, in the PNA+ months than in PNA–
457 months (Table 2). The simulated relative difference in $PM_{2.5}$ was close to that from
458 observations (Table 1) in the western U.S., but the simulated relative differences in
459 $PM_{2.5}$ were larger than those from observations in the eastern and whole of U.S..

460 Fig. 5 also shows the differences in simulated surface-layer concentrations of
461 SO_4^{2-}, NO_3^- and NH_4^+ between the PNA+ and the PNA– months. The differences in
462 concentrations of SO_4^{2-} were larger in the western than in the eastern U.S., with
463 maximum enhancements of 0.4–0.8 μg m^{-3} (30–50%) over the West North Central
464 States (South Dakota, Nebraska, Minnesota, Iowa, and Missouri). The differences in
465 concentrations of NO_3^- and NH_4^+ between PNA+ and PNA– months had similar
466 geographical patterns, with increases in concentrations in a large fraction of the
467 eastern U.S. and over a belt region along the Rocky Mountain in the western U.S..
468 The increases in concentrations of NO_3^- and NH_4^+ over the eastern U.S. in PNA+
469 months relative to PNA– months agreed very well with those seen in observations in
470 most regions of the U.S. (Fig. 3). The model underestimates the differences in NO_3^-
471 in California and the southeastern U.S., because the model does not capture well the
472 temporal variations of NO_3^- in these two regions (Fig. S4). The differences in

473 concentrations of SO_4^{2-}, NO_3^- and NH_4^+ in the eastern U.S. between the PNA+ and
474 PNA– months were 0.2 μg m^{-3} (4.0%), 0.4 μg m^{-3} (33.5%), and 0.2 μg m^{-3} (13.2%),
475 respectively (Table 2).

476 The differences in concentrations of OC and BC between PNA+ and PNA–
477 months had similar geographical patterns, with large increases in concentrations over
478 and near the eastern Midwest and the region from northwestern U.S. to Texas. The
479 maximum differences reached 0.2–0.4 μg m^{-3} (10–20%) and 0.1–0.2 μg m^{-3} (20–
480 30%) in Illinois, Indiana and Ohio for OC and BC, respectively. The magnitudes of the
481 differences in OC and BC were statistically significant but were smaller than the
482 observations (Tables 1 and 2). The absolute differences in OC were less than 0.1 μg
483 m^{-3} in the western, eastern and whole of U.S due to the underestimation of OC in the
484 simulation.

485 In summary, model results agreed with observations in that the concentrations of
486 all aerosol species of SO_4^{2-}, NO_3^-, NH_4^+, BC, and OC averaged over the U.S. were
487 higher in PNA+ months than in PNA– months. Relative to the PNA– months, the
488 average concentration of $PM_{2.5}$ over the U.S. was higher by about 8.7% (12.2%)
489 based on observed (simulated) concentrations. Furthermore, simulated geographical
490 patterns of the differences in $PM_{2.5}$ and each aerosol species between the PNA+ and
491 PNA– months were similar to those seen in observations in most areas of the U.S.
492 (except for California), with the largest increases in aerosol concentrations in PNA+
493 months over and near the eastern Midwest.
494

5 Mechanisms for the impact of PNA on aerosol concentrations

5.1 The impact of PNA on transboundary transport of aerosols

The transboundary transport of pollutants to and from the U.S. depends largely on winds in the free troposphere (Liang et al. 2004). Figure 6 shows the horizontal winds at 700 hPa averaged over the winter months of NDJFM of 1986–2006 and the corresponding differences between PNA+ and PNA– months on the basis of the GEOS-4 meteorological fields. Strong westerlies prevailed over the U.S. in wintertime (Fig. 6a). Relative to the PNA– months, anomalous northeasterlies occurred over a large fraction of U.S. in the PNA+ months. Anomalous anti-cyclonic circulation occurred near the northwestern U.S. and anomalous cyclonic circulation occurred near the southeastern U.S. (Fig. 6b), corresponding to the large positive and negative differences in geopotential height in these two regions (see auxiliary Fig. S1), respectively.

We also calculate mass fluxes of $PM_{2.5}$ at the four lateral boundaries (from the surface to 250 hPa) of the U. S. for different PNA phases (Table 3). The domain of the box to represent the U. S. is (75–120°W, 28–49°N), as shown in Fig. 6b. For $PM_{2.5}$ in wintertime, the inflow from the west boundary and the outflow from the east boundary had the largest absolute values (Table 3). Relative to the PNA– months, the inflow from the west boundary and the outflow from the east boundary in PNA+ months exhibited reductions of 16.1 kg s^{-1} and 13.5 kg s^{-1}, respectively (Table 3). The inflow flux from south boundary decreased by 15.8 kg s^{-1}, and the inflow flux from north boundary increased by 31.7 kg s^{-1}, leading to a net increase of inflow flux of 13.3 kg s^{-1} in PNA+ months. Therefore, the transboundary transport has an overall effect of increasing $PM_{2.5}$ aerosols in the U.S. in PNA+ months relative to PNA– months. The relative change in net flux was 9.9% ((PNA+ minus PNA–)·100%/PNA–) (Table 3),

coinciding well with the enhancement of 12.2% in surface-layer $PM_{2.5}$ concentration averaged over the U.S. (Table 2). Note that because the GEOS-Chem model underestimates $PM_{2.5}$ concentrations in the western U.S. (Fig. 4b), the net outflow flux from the selected box might have been underestimated, but this should not compromise our conclusions about the relative differences in net flux between PNA+ and PNA– phases.

5.2 Local changes in aerosol concentrations caused by the PNA

The PNA pattern is also associated with variations in meteorological variables such as temperature (Leathers et al. 1991; Konrad II 1998; Notaro et al. 2006; Knight et al. 2008; Liu et al. 2015; Ning and Bradley 2014, 2015), precipitation (Leathers et al. 1991; Henderson and Robinson 1994; Coleman and Rogers 2003; Notaro et al. 2006; Archambault et al. 2008; Myoung and Deng 2009; Ning and Bradley 2014, 2015; Wise et al. 2015) and humidity (Sheridan 2003; Coleman and Rogers 2003; Knight et al. 2008) in U.S.，which are expected to influence aerosol concentrations within the U.S. through chemical reactions, transport, and deposition.

Figure 7 shows the composite differences, between the PNA+ and PNA– months, in surface air temperature (T), precipitation rate (PR), relative humidity (RH), surface wind speed (WS), and planetary boundary layer height (PBLH), based on the reanalyzed GEOS-4 datasets. Relative to PNA– months, temperatures were higher by 1–3 K over the northwestern U.S. and lower by 1–4 K in the southeastern region. Such geographic distributions of temperature anomalies were attributed to the maritime warm air in the northwestern U.S. accompanied by the enhanced tropospheric geopotential height in North America (Leathers et al. 1991; Sheridan 2003; Liu et al. 2015; Ning and Bradley 2015) (see also auxiliary Fig. 1d) and the more frequent outbreak of cold air in southeastern U.S. accompanied by the

depressed geopotential height (Konrad II 1998; Liu et al. 2015) (see also auxiliary Fig. 1d). The differences in precipitation between PNA+ and PNA– months reached –1.6 to –2.4 mm day^{-1} (–32 to –48%) over and near the eastern Midwest, –2.4 to –3.2 mm day^{-1} (–48 to –64%) in the northwestern U.S., and 1.6–2.4 mm day^{-1} (16–32%) in the southeastern U.S.. These effects of PNA on precipitation were similar to those obtained from wintertime station data by Leathers et al. (1991), Coleman and Rogers (2003) and Wise et al. (2015). With respect to RH, the values in the eastern U.S. were generally lower in the PNA+ months than in PNA– months, as a result of the reduced moisture flux from the Gulf of Mexico to the eastern U.S. (Coleman and Rogers 2003), where RH showed maximum reduction of –3 to –9%. The enhancement of RH of up to 6–9% in Texas, Oklahoma and New Mexico was due to the anomalous easterlies over the south central U.S. (see Fig. 7), which diminished the influence of the dry air from the deserts of the southwestern U.S. and northwestern Mexico in PNA+ months (Sheridan 2003). The surface WS showed reductions in PNA+ months relative to PNA– months in two regions, one was the belt region along the Rocky Mountain from the northwestern U.S. to Texas (with the maximum reductions of 1.5–2.0 m s^{-1} (48–64%)) and the other region, with a northeast-southwest orientation, was from Ohio to Louisiana (with maximum reductions of 0.5–1.0 m s^{-1} (16–32%)). The differences in PBLH between PNA+ and PNA– months were statistically significant in the western U.S. and in the belt region from the northeastern U.S. to the eastern Midwest, with the maximum reductions in PBLH of 75–100 m (15–20%) and 75–100 m (10–15%), respectively. The changes of PBLH were possibly associated with the frequent outbreak of cold air in the U.S. in PNA+ phases (Leathers et al., 1991; Archambault et al., 2010), which induced cool air at the surface and clouds over the intermountain and the eastern Midwest regions (Sheridan, 2003).

570 The comparisons of Fig. 5b with Fig. 7a indicate that the increases in $PM_{2.5}$
571 concentrations over and near the eastern Midwest in PNA+ months relative to the
572 PNA– months can be attributed to the decreases in PR, WS and PBLH in these
573 locations, since the changes in these three variables depressed wet deposition, local
574 horizontal diffusion, and vertical diffusion of the surface aerosols, respectively. The
575 increases in SO_4^{2-} in the western U.S. (Fig. 5b) corresponded to the decreases in PR
576 and PBLH and the increased temperature. The increases in temperature enhance
577 chemical reaction rates (Aw and Kleeman 2003; Dawson et al. 2007; Kleeman 2008).
578 In the eastern U.S., although PR, WS, and PBLH decreased over and near the
579 eastern Midwest, the cooling in the eastern U.S. might have offset the effects by PR,
580 WS, and PBLH, inducing practically no changes in SO_4^{2-} in the eastern U.S.. The
581 large increases in NO_3^- and NH_4^+ in the southeastern U.S. (Fig. 5b) can be attributed
582 to the reduced surface temperature, which was favorable to the wintertime formation
583 of NO_3^- and NH_4^+ (Dawson et al. 2007). The differences in concentrations of OC and
584 BC between PNA+ and PNA– corresponded well with the reduced PR, WS and
585 PBLH.
586 In order to quantify the impacts of anomalies in meteorological parameters driven
587 by PNA on concentrations of different aerosol species, the pattern correlation
588 coefficients (PCC, http://glossary.ametsoc.org/wiki/Pattern_correlation) are
589 calculated and shown in Table 4. These pattern correlation coefficients denote the
590 relationship between the geographical distribution of anomalies of each of T, PR, RH,
591 WS, and PBLH (Fig. 7b) and that of the differences in concentration of each aerosol
592 species between PNA+ and PNA– months (Fig. 5c). As shown in Table 4, over the
593 whole U.S., the PNA influenced SO_4^{2-} concentrations mainly through changes PBLH,
594 PR, and T, with the highest PCC values of –0.43, –0.38, and +0.26, respectively. For

595 NO_3^-, the PNA-induced variations in temperature had a strong negative correlation
596 (PCC=–0.59) with the PNA-induced differences in concentrations, indicating that
597 surface temperature was the dominant meteorological factor to influence NO_3^-
598 concentrations. For NH_4^+, OC, and BC, PR and PBLH were the two variables that had
599 the largest negative PCC values (Table 4).
600

601 **6 Conclusions**

602 This study examined the impacts of monthly variation in the PNA phase on wintertime
603 surface-layer aerosol concentrations in the U.S. by the analyses of EPA-AQS
604 observations over 1999–2013 and model results for 1986–2006 from the global
605 chemical transport model GEOS-Chem.

606 The composite analyses on the EPA-AQS observations showed that the average
607 concentrations of $PM_{2.5}$, SO_4^{2-}, NO_3^-, NH_4^+, OC, and BC aerosols over the U.S. were
608 higher in the PNA+ months than in the PNA– months by 1.0 μg m^{-3} (8.7%), 0.01 μg
609 m^{-3} (0.5%), 0.3 μg m^{-3} (29.1%), 0.1 μg m^{-3} (11.9%), 0.6 μg m^{-3} (13.5%), and 0.2 μg
610 m^{-3} (27.8%), respectively. Regionally, the observed $PM_{2.5}$ concentrations were higher
611 by 3–5 μg m^{-3} (40–80%) over the Midwest, and by 7–9 μg m^{-3} (80–100%) around the
612 Salt Lake, as the concentrations in PNA+ months were compared to those in PNA–
613 months.

614 The impacts of PNA phase on aerosol concentrations were reproduced fairly well
615 by the GEOS-Chem simulation with fixed anthropogenic emissions (the variations of
616 aerosols concentrations were driven by changes in meteorological fields alone).
617 Concentrations of SO_4^{2-}, NO_3^-, NH_4^+, BC, and OC averaged over the U.S. were
618 simulated to be higher in the PNA+ months than in PNA– months. The average
619 concentration of $PM_{2.5}$ over the U.S. was simulated to be 12.2% higher in the PNA+

620 months relative to the PNA– months, in close agreement with the observations.
621 Simulated geographical patterns of the differences in $PM_{2.5}$ and each aerosol species
622 between the PNA+ and PNA– months were similar to those seen in observations. The
623 largest increases in aerosol concentrations in the PNA+ months were simulated to be
624 over and near the eastern Midwest, but the model results showed small PNA-induced
625 changes in aerosol concentrations in the western U.S..

626 The mechanisms for the impacts of PNA on aerosol concentrations were
627 examined. The transboundary transport was found to have an overall effect of
628 increasing $PM_{2.5}$ aerosols in the U.S. in the PNA+ months relative to PNA– months.
629 Compared to the PNA– months, anomalous northeasterlies occurred over a large
630 fraction of U.S., which led to a net increase in inflow flux of $PM_{2.5}$ of 14.0 Kg s^{-1} in
631 PNA+ months. Regionally within the U.S., the PNA influenced aerosol concentrations
632 through changes in precipitation rate (PR), planetary boundary layer height (PBLH),
633 surface wind speed (WS), surface air temperature (T) and relative humidity (RH), as
634 represented by the pattern correlation coefficients (PCCs). The PNA influenced SO_4^{2-}
635 concentration mainly through changes PBLH, PR, and T, with the highest PCC values
636 of –0.43, –0.38, and +0.26, respectively. For NO_3^-, the PNA-induced variations in
637 temperature had a strong negative correlation (PCC=–0.59) with the PNA-induced
638 differences in concentrations. For NH_4^+, OC, and BC, PR and PBLH were the two
639 variables that had the largest negative PCC values. It should be noted that, the PCC
640 values only statistically present the relationship between meteorological parameters
641 and aerosol concentrations in the U.S.. More in-depth understanding of the impact of
642 PNA phase on aerosol concentrations should be carried out on the basis of physical
643 and chemical processes.

644 Conclusions from this study have important implications for air quality in the U.S..
645 Leathers and Palechi (1992) showed that the PNAI were generally low in 1947–1957
646 but consistently high in 1958–1987. The PNAI during 1948–2010 exhibited an
647 increasing trend for positive phases and a decreasing trend for negative phases (Liu
648 et al. 2015; Ning et al. 2015; http://research.jisao.washington.edu/data_sets/pna/#djf),
649 indicating that wintertime particulate matter pollution in most areas of U.S.
650 deteriorated due to variations in PNA phase alone. Climate models projected that
651 positive PNA phases would increase in the future because of the global warming
652 (Kachi and Nitta, 1997; Müller and Roeckner 2008; Zhou 2014). Therefore, the trend
653 in PNA pattern underlies the necessity of strict emission reduction strategies for
654 greenhouse gases, aerosols, and aerosol precursors.
655
656
657 *Acknowledgements.* This work was supported by the National Basic Research
658 Program of China (973 program, Grant 2014CB441202), the Strategic Priority
659 Research Program of the Chinese Academy of Sciences Strategic Priority Research
660 Program Grant No. XDA05100503, and the National Natural Science Foundation of
661 China under grants 91544219, 41475137, and 41321064.
662

663 **References**

664 Alexander, B., Park, R.J., Jacob, D.J., Li, Q.B., Yantosca, R.M., Savarino, J., Lee,
665 C.C.W., Thiemens, M.H.: Sulfate formation in sea-salt aerosols: Constraints from
666 oxygen isotopes, J. Geophys. Res., 110(D10), D10307,
667 doi:10.1029/2004JD005659, 2005.

668 Allen, R. J., Landuyt, W. and Rumbold, S. T.: An increase in aerosol burden and
669 radiative effects in a warmer world, Nat. Clim. Chang., (OCTOBER),
670 doi:10.1038/nclimate2827, 2015.

671 Alston, E. J., Sokolik, I. N. and Kalashnikova, O. V.: Characterization of atmospheric
672 aerosol in the US Southeast from ground- and space-based measurements over
673 the past decade, Atmos. Meas. Tech., 5(7), 1667–1682,
674 doi:10.5194/amt-5-1667-2012, 2012.

675 Archambault, H. M., Bosart, L. F., Keyser, D. and Aiyyer, A. R.: Influence of
676 Large-Scale Flow Regimes on Cool-Season Precipitation in the Northeastern
677 United States, Mon. Weather Rev., 136(8), 2945–2963,
678 doi:10.1175/2007MWR2308.1, 2008.

679 Athanasiadis, P. J. and Ambaum, M. H. P.: Linear Contributions of Different Time
680 Scales to Teleconnectivity, J. Clim., 22(13), 3720–3728,
681 doi:10.1175/2009JCLI2707.1, 2009.

682 Aw, J. and Kleeman, M. J.: Evaluating the first-order effect of intraannual temperature
683 variability on urban air pollution, J. Geophys. Res., 108(D12), 4365,
684 doi:10.1029/2002JD002688, 2003.

685 Bauer, S. E., Koch, D., Unger, N., Metzger, S. M., Shindell, D. T. and Streets, D. G.:
686 Nitrate aerosols today and in 2030: a global simulation including aerosols and
687 tropospheric ozone, Atmos. Chem. Phys., 7(19), 5043–5059,
688 doi:10.5194/acp-7-5043-2007, 2007.

689 Bey, I., Jacob, D. J., Yantosca, R. M., Logan, J. a., Field, B. D., Fiore, A. M., Li, Q., Liu,
690 H. Y., Mickley, L. J. and Schultz, M. G.: Global modeling of tropospheric
691 chemistry with assimilated meteorology: Model description and evaluation, J.
692 Geophys. Res., 106(D19), 23073, doi:10.1029/2001JD000807, 2001.

693 Blackmon, M. L., Lee, Y.-H. and Wallace, J. M.: Horizontal Structure of 500 mb Height
694 Fluctuations with Long, Intermediate and Short Time Scales, J. Atmos. Sci.,
695 41(6), 961–980, doi:10.1175/1520-0469(1984)041<0961:HSOMHF>2.0.CO;2,
696 1984.

697 Cakmur, R. V., Miller, R. L. and Tegen, I.: A comparison of seasonal and interannual
698 variability of soil dust aerosols over the Atlantic Ocean as inferred by the TOMS
699 AI and AVHRR AOT retrievals, J. Geophys. Res., 106(D16), 18287,
700 doi:10.1029/2000JD900525, 2001.

701 Chen, J., Vaughan, J., Avise, J., O'Neill, S. and Lamb, B.: Enhancement and
702 evaluation of the AIRPACT ozone and $PM_{2.5}$ forecast system for the Pacific
703 Northwest, J. Geophys. Res. Atmos., 113(14), 1–20,
704 doi:10.1029/2007JD009554, 2008.

705 Coleman, J. S. M. and Rogers, J. C.: Ohio River Valley Winter Moisture Conditions
706 Associated with the Pacific–North American Teleconnection Pattern, J. Clim.,

16(6), 969–981, doi:10.1175/1520-0442(2003)016<0969:ORVWMC>2.0.CO;2, 2003.

Dawson, J. P., Adams, P. J. and Pandis, S. N.: Sensitivity of $PM_{2.5}$ to climate in the Eastern US: a modeling case study, Atmos. Chem. Phys., 7(16), 4295–4309, doi:10.5194/acp-7-4295-2007, 2007.

Day, M. C. and Pandis, S. N.: Predicted changes in summertime organic aerosol concentrations due to increased temperatures, Atmos. Environ., 45(36), 6546–6556, doi:10.1016/j.atmosenv.2011.08.028, 2011.

Di Pierro, M., Jaeglé, L. and Anderson, T. L.: Satellite observations of aerosol transport from East Asia to the Arctic: three case studies, Atmos. Chem. Phys., 11(5), 2225–2243, doi:10.5194/acp-11-2225-2011, 2011.

Drury, E., Jacob, D. J., Spurr, R. J. D., Wang, J., Shinozuka, Y., Anderson, B. E., Clarke, A. D., Dibb, J., McNaughton, C. and Weber, R.: Synthesis of satellite (MODIS), aircraft (ICARTT), and surface (IMPROVE, EPA-AQS, AERONET) aerosol observations over eastern North America to improve MODIS aerosol retrievals and constrain surface aerosol concentrations and sources, J. Geophys. Res., 115(D14), D14204, doi:10.1029/2009JD012629, 2010.

Duncan, B. N., Martin, R. V., Staudt, A. C., Yevich, R. and Logan, J. A.: Interannual and seasonal variability of biomass burning emissions constrained by satellite observations, J. Geophys. Res., 108(D2), 4100, doi:10.1029/2002JD002378, 2003.

Dutkiewicz, V. A., Das, M. and Husain, L.: The relationship between regional SO2 emissions and downwind aerosol sulfate concentrations in the northeastern US, Atmos. Environ., 34(11), 1821–1832, doi:10.1016/S1352-2310(99)00334-9, 2000.

Fairlie, D. T., Jacob, D. J. and Park, R. J.: The impact of transpacific transport of mineral dust in the United States, Atmos. Environ., 41(6), 1251–1266, doi:10.1016/j.atmosenv.2006.09.048, 2007.

Feldstein, S. B.: Fundamental mechanisms of the growth and decay of the PNA teleconnection pattern, Q. J. R. Meteorol. Soc., 128(581), 775–796, doi:10.1256/0035900021643683, 2002.

Feldstein, S. B.: The dynamics of NAO teleconnection pattern growth and decay, Q. J. R. Meteorol. Soc., 129(589), 901–924, doi:10.1256/qj.02.76, 2003.

Fu, T.-M., Jacob, D. J. and Heald, C. L.: Aqueous-phase reactive uptake of dicarbonyls as a source of organic aerosol over eastern North America, Atmos. Environ., 43(10), 1814–1822, doi:10.1016/j.atmosenv.2008.12.029, 2009.

Generoso, S., Bréon, F.-M., Balkanski, Y., Boucher, O. and Schulz, M.: Improving the seasonal cycle and interannual variations of biomass burning aerosol sources, Atmos. Chem. Phys., 3(4), 1211–1222, doi:10.5194/acp-3-1211-2003, 2003.

Giglio, L., van der Werf, G. R., Randerson, J. T., Collatz, G. J. and Kasibhatla, P.: Global estimation of burned area using MODIS active fire observations, Atmos. Chem. Phys., 6(4), 957–974, doi:10.5194/acp-6-957-2006, 2006.

Gong, S. L., Zhang, X. Y., Zhao, T. L., Zhang, X. B., Barrie, L. A., McKendry, I. G. and Zhao, C. S.: A Simulated Climatology of Asian Dust Aerosol and Its Trans-Pacific

751 Transport. Part II: Interannual Variability and Climate Connections, J. Clim.,
752 19(1), 104–122, doi:10.1175/JCLI3606.1, 2006.

753 Guenther, A., Karl, T., Harley, P., Wiedinmyer, C., Palmer, P. I. and Geron, C.:
754 Estimates of global terrestrial isoprene emissions using MEGAN (Model of
755 Emissions of Gases and Aerosols from Nature), Atmos Chem Phys 6:3181-3210.
756 doi: 10.5194/acp-6-3181-2006, 2006.

757 Hack, J. J.: Parameterization of moist convection in the National Center for
758 Atmospheric Research community climate model (CCM2), J. Geophys. Res.,
759 99(D3), 5551, doi:10.1029/93JD03478, 1994.

760 Hand, J. L., Schichtel, B. A., Malm, W. C. and Pitchford, M. L.: Particulate sulfate ion
761 concentration and SO_2 emission trends in the United States from the early 1990s
762 through 2010, Atmos. Chem. Phys., 12(21), 10353–10365,
763 doi:10.5194/acp-12-10353-2012, 2012a.

764 Hand, J. L., Schichtel, B. A., Pitchford, M., Malm, W. C. and Frank, N. H.: Seasonal
765 composition of remote and urban fine particulate matter in the United States, J.
766 Geophys. Res., 117(D5), D05209, doi:10.1029/2011JD017122, 2012b.

767 Hand, J. L., Schichtel, B. A., Malm, W. C., Pitchford, M. and Frank, N. H.: Spatial and
768 seasonal patterns in urban influence on regional concentrations of speciated
769 aerosols across the United States, J. Geophys. Res. Atmos., 119, 12832–
770 12849, doi:10.1002/2014JD022328.Received, 2014.

771 Heald, C. L., Jacob, D. J., Park, R. J., Alexander, B., Fairlie, T. D., Yantosca, R. M. and
772 Chu, D. A.: Transpacific transport of Asian anthropogenic aerosols and its impact
773 on surface air quality in the United States, J. Geophys. Res. D Atmos., 111, 1–13,
774 doi:10.1029/2005JD006847, 2006.

775 Heald, C. L., Henze, D. K., Horowitz, L. W., Feddema, J., Lamarque, J.-F., Guenther,
776 A., Hess, P. G., Vitt, F., Seinfeld, J. H., Goldstein, A. H. and Fung, I.: Predicted
777 change in global secondary organic aerosol concentrations in response to future
778 climate, emissions, and land use change, J. Geophys. Res. Atmos., 113(D5),
779 D05211, doi:10.1029/2007JD009092, 2008.

780 Heald, C. L., J. L. Collett Jr., Lee, T., Benedict, K. B., Schwandner, F. M., Li, Y.,
781 Clarisse, L., Hurtmans, D. R., Van Damme, M., Clerbaux, C., Coheur, P.-F.,
782 Philip, S., Martin, R. V. and Pye, H. O. T.: Atmospheric ammonia and particulate
783 inorganic nitrogen over the United States, Atmos. Chem. Phys., 12(21), 10295–
784 10312, doi:10.5194/acp-12-10295-2012, 2012.

785 Henderson, K. G. and Robinson, P. J.: Relationships between the pacific/north
786 american teleconnection patterns and precipitation events in the south-eastern
787 USA, Int. J. Climatol., 14(3), 307–323, doi:10.1002/joc.3370140305, 1994.

788 Holmes, C. D., Prather, M. J., Søvde, O. A. and Myhre, G.: Future methane, hydroxyl,
789 and their uncertainties: key climate and emission parameters for future
790 predictions, Atmos. Chem. Phys., 13(1), 285–302, doi:10.5194/acp-13-285-2013,
791 2013.

792 IPCC: Climate Change 2013 The Physical Science Basis: Working Group I
793 Contribution to the Fifth Assessment Report of the Intergovernmental Panel on
794 Climate Change, 1st ed., Cambridge University Press, New York. [online]
795 Available from:

http://www.climatechange2013.org/images/report/WG1AR5_ALL_FINAL.pdf" The last access date was November 20, 2015.

Jacob, D. J. and Winner, D. A.: Effect of climate change on air quality, Atmos. Environ., 43(1), 51–63, doi:10.1016/j.atmosenv.2008.09.051, 2009.

Jaffe, D., Tamura, S. and Harris, J.: Seasonal cycle and composition of background fine particles along the west coast of the US, Atmos. Environ., 39(2), 297–306, doi:10.1016/j.atmosenv.2004.09.016, 2005.

Jerez, S., Jimenez-Guerrero, P., Montávez, J. P. and Trigo, R. M.: Impact of the North Atlantic Oscillation on European aerosol ground levels through local processes: a seasonal model-based assessment using fixed anthropogenic emissions, Atmos. Chem. Phys., 13(22), 11195–11207, doi:10.5194/acp-13-11195-2013, 2013.

Juda-Rezler, K., Reizer, M., Huszar, P., Krüger, B., Zanis, P., Syrakov, D., Katragkou, E., Trapp, W., Melas, D., Chervenkov, H., Tegoulias, I. and Halenka, T.: Modelling the effects of climate change on air quality over Central and Eastern Europe: concept, evaluation and projections, Clim. Res., 53(3), 179–203, doi:10.3354/cr01072, 2012.

Kachi, M. and Nitta, T.: Decadal variations of the global atmosphere-ocean system, J. Meteorol. Soc. Japan, 75(3), 657–675, 1997.

Kleeman, M. J.: A preliminary assessment of the sensitivity of air quality in California to global change, Clim. Change, 87(1), 273–292, doi:10.1007/s10584-007-9351-3, 2008.

Knight, D. B., Davis, R. E., Sheridan, S. C., Hondula, D. M., Sitka, L. J., Deaton, M., Lee, T. R., Gawtry, S. D., Stenger, P. J., Mazzei, F. and Kenny, B. P.: Increasing frequencies of warm and humid air masses over the conterminous United States from 1948 to 2005, Geophys. Res. Lett., 35(10), L10702, doi:10.1029/2008GL033697

Konrad II, C. E.: Persistent planetary scale circulation patterns and their relationship with cold air outbreak activity over the Eastern United States, Int. J. Climatol., 18(11), 1209–1221, doi:10.1002/(SICI)1097-0088(199809)18:11<1209::AID-JOC301>3.0.CO;2-K, 1998.

Lam, Y. F., Fu, J. S., Wu, S. and Mickley, L. J.: Impacts of future climate change and effects of biogenic emissions on surface ozone and particulate matter concentrations in the United States, Atmos. Chem. Phys., 11(10), 4789–4806, doi:10.5194/acp-11-4789-2011, 2011.

Leathers, D. J. and Palecki, M. A.: The Pacific/North American Teleconnection Pattern and United States Climate. Part II: Temporal Characteristics and Index Specification, J. Clim., 5(7), 707–716, doi:10.1175/1520-0442(1992)005<0707:TPATPA>2.0.CO;2, 1992.

Leathers, D. J., Yarnal, B. and Palecki, M. A.: The Pacific/North American Teleconnection Pattern and United States Climate. Part I: Regional Temperature and Precipitation Associations, J. Clim., 4(5), 517–528, doi:10.1175/1520-0442(1991)004<0517:TPATPA>2.0.CO;2, 1991.

Leibensperger, E. M., Mickley, L. J., Jacob, D. J. and Barrett, S. R. H.: Intercontinental influence of NO_x and CO emissions on particulate matter air quality, Atmos. Environ., 45(19), 3318–3324, doi:10.1016/j.atmosenv.2011.02.023, 2011.

Li, J., Carlson, B. E. and Lacis, A. A.: Application of spectral analysis techniques in the intercomparison of aerosol data: 1. An EOF approach to analyze the spatial-temporal variability of aerosol optical depth using multiple remote sensing data sets, J. Geophys. Res. Atmos., 118(15), 8640–8648, doi:10.1002/jgrd.50686, 2013.

Liang, Q., Jaeglé, L., Jaffe, D. A., Weiss-Penzias, P., Heckman, A. and Snow, J. A.: Long-range transport of Asian pollution to the northeast Pacific: Seasonal variations and transport pathways of carbon monoxide, J. Geophys. Res. D Atmos., 109, 1–16, doi:10.1029/2003JD004402, 2004.

Liang, Q., Jaeglé, L. and Wallace, J. M.: Meteorological indices for Asian outflow and transpacific transport on daily to interannual timescales, J. Geophys. Res., 110(D18), D18308, doi:10.1029/2005JD005788, 2005.

Liao, H., Chen, W. T. and Seinfeld, J. H.: Role of climate change in global predictions of future tropospheric ozone and aerosols, J. Geophys. Res. Atmos., 111, 1–18, doi:10.1029/2005JD006852, 2006.

Liao, H., Henze, D. K., Seinfeld, J. H., Wu, S. and Mickley, L. J.: Biogenic secondary organic aerosol over the United States: Comparison of climatological simulations with observations, J. Geophys. Res., 112(D6), D06201, doi:10.1029/2006JD007813, 2007.

Lin, S.-J. and Rood, R. B.: Multidimensional Flux-Form Semi-Lagrangian Transport Schemes, Mon. Weather Rev., 124(9), 2046–2070, doi:10.1175/1520-0493(1996)124<2046:MFFSLT>2.0.CO;2, 1996.

Liu, H.-Y., Jacob, D. J., Bey, I. and Yantosca, R. M.: Constraints Pb-210 and Be-7 on Wet Deposition and Transport in a Global Three-Dimensional Chemical Tracer Model Driven by Assimilated Meteorological Fields, J. Geophys. Res. Atmos., 106(Dll), doi:10.1029/2000JD900839, 2001.

Liu, Y., Park, R. J., Jacob, D. J., Li, Q., Kilaru, V. and Sarnat, J. A.: Mapping annual mean ground-level $PM_{2.5}$ concentrations using Multiangle Imaging Spectroradiometer aerosol optical thickness over the contiguous United States, J. Geophys. Res., 109(D22), D22206, doi:10.1029/2004JD005025, 2004.

Liu, Y., Liu, J. and Tao, S.: Interannual variability of summertime aerosol optical depth over East Asia during 2000–2011: a potential influence from El Niño Southern Oscillation, Environ. Res. Lett., 8(4), 044034, doi:10.1088/1748-9326/8/4/044034, 2013.

Liu, Z., Jian, Z., Yoshimura, K., Buenning, N. H., Poulsen, C. J. and Bowen, G. J.: Recent contrasting winter temperature changes over North America linked to enhanced positive Pacific-North American pattern, Geophys. Res. Lett., 42, 1–8, doi:10.1002/2015GL065656, 2015.

Mahowald, N., Luo, C., del Corral, J., Zender, C.S.: Interannual variability in atmospheric mineral aerosols from a 22-year model simulation and observational data, J. Geophys. Res., 108(D12), 4352, doi:10.1029/2002JD002821, 2003.

885 Malm, W. C.: Spatial and monthly trends in speciated fine particle concentration in the
886 United States, J. Geophys. Res., 109(D3), D03306, doi:10.1029/2003JD003739,
887 2004.

888 Malm, W. C., Schichtel, B. A. and Pitchford, M. L.: Uncertainties in $PM_{2.5}$ Gravimetric
889 and Speciation Measurements and What We Can Learn from Them, J. Air Waste
890 Manage. Assoc., 61(11), 1131–1149, doi:10.1080/10473289.2011.603998,
891 2011.

892 Markakis, K., Valari, M., Perrussel, O., Sanchez, O. and Honore, C.: Climate-forced
893 air-quality modeling at the urban scale: sensitivity to model resolution, emissions
894 and meteorology, Atmos. Chem. Phys., 15(13), 7703–7723,
895 doi:10.5194/acp-15-7703-2015, 2015.

896 Megaritis, a. G., Fountoukis, C., Charalampidis, P. E., Denier van der Gon, H. a. C.,
897 Pilinis, C. and Pandis, S. N.: Linking climate and air quality over Europe: effects
898 of meteorology on $PM_{2.5}$ concentrations, Atmos. Chem. Phys., 14(18), 10283–
899 10298, doi:10.5194/acp-14-10283-2014, 2014.

900 Mijling, B., van der A, R. J. and Zhang, Q.: Regional nitrogen oxides emission trends in
901 East Asia observed from space, Atmos. Chem. Phys., 13, 12003-12012, doi:
902 10.5194/acp-13-12003-2013, 2013.

903 Moulin, C. and Lambert, C. E., Dulac, F., Dayan, U.: Control of atmospheric export of
904 dust from North Africa by the North Atlantic Oscillation, Nature, 387(June), 691–
905 694, 1997.

906 Mu, Q. and Liao, H.: Simulation of the interannual variations of aerosols in China: role
907 of variations in meteorological parameters, Atmos. Chem. Phys., 14, 11177–
908 11219, doi:10.5194/acp-14-9597-2014, 2014.

909 Müller, W. A. and Roeckner, E.: ENSO teleconnections in projections of future climate
910 in ECHAM5/MPI-OM, Clim. Dyn., 31(5), 533–549,
911 doi:10.1007/s00382-007-0357-3, 2008.

912 Murray, L. T., Jacob, D. J., Logan, J. A., Hudman, R. C. and Koshak, W. J.: Optimized
913 regional and interannual variability of lightning in a global chemical transport
914 model constrained by LIS/OTD satellite data, J. Geophys. Res. Atmos.,
915 117(D20), D20307, doi:10.1029/2012JD017934, 2012.

916 Myoung, B. and Deng, Y.: Interannual Variability of the Cyclonic Activity along the U.S.
917 Pacific Coast: Influences on the Characteristics of Winter Precipitation in the
918 Western United States, J. Clim., 22(21), 5732–5747,
919 doi:10.1175/2009JCLI2889.1, 2009.

920 Ning, L. and Bradley, R. S.: Winter precipitation variability and corresponding
921 teleconnections over the northeastern United States, J. Geophys. Res. Atmos.,
922 119(13), 7931–7945, doi:10.1002/2014JD021591, 2014.

923 Ning, L. and Bradley, R. S.: Winter Climate Extremes over the Northeastern United
924 States and Southeastern Canada and Teleconnections with Large-Scale Modes
925 of Climate Variability, J. Clim., 28(6), 2475–2493,
926 doi:10.1175/JCLI-D-13-00750.1, 2015.

927 Notaro, M., Wang, W.-C. and Gong, W.: Model and Observational Analysis of the
928 Northeast U.S. Regional Climate and Its Relationship to the PNA and NAO

Patterns during Early Winter, Mon. Weather Rev., 134(11), 3479–3505, doi:10.1175/MWR3234.1, 2006.

Park, R. J., Jacob, D. J., Chin, M., Martin, R. V.: Sources of carbonaceous aerosols over the United States and implications for natural visibility, J. Geophys. Res., 108(D12), 4355, doi:10.1029/2002JD003190, 2003.

Park, R. J., Jacob, D. J., Field, B. D., Yantosca, R. M., Chin, M.: Natural and transboundary pollution influences on sulfate-nitrate-ammonium aerosols in the United States: Implications for policy, J. Geophys. Res., 109(D15), D15204, doi:10.1029/2003JD004473, 2004.

Park, R. J., Jacob, D. J., Palmer, P. I., Clarke, A. D., Weber, R. J., Zondlo, M. A., Eisele, F. L., Bandy, A. R., Thornton, D. C., Sachse, G. W. and Bond, T. C.: Export efficiency of black carbon aerosol in continental outflow: Global implications, J. Geophys. Res. Atmos., 110, 1–7, doi:10.1029/2004JD005432, 2005.

Park, R. J., Jacob, D. J., Kumar, N. and Yantosca, R. M.: Regional visibility statistics in the United States: Natural and transboundary pollution influences, and implications for the Regional Haze Rule, Atmos. Environ., 40(28), 5405–5423, doi:10.1016/j.atmosenv.2006.04.059, 2006.

Porter, W. C., Heald, C. L., Cooley, D. and Russell, B.: Investigating the observed sensitivities of air-quality extremes to meteorological drivers via quantile regression, Atmos. Chem. Phys., 15(18), 10349–10366, doi:10.5194/acp-15-10349-2015, 2015.

Prather, M., Holmes, C., and Hsu, J.: Reactive greenhouse gas scenarios: Systematic exploration of uncertainties and the role of atmospheric chemistry, Geophys. Res. Lett., 39, doi:10.1029/2012GL051440, 2012.

Pye, H. O. T., Liao, H., Wu, S., Mickley, L. J., Jacob, D. J., Henze, D. K. and Seinfeld, J. H.: Effect of changes in climate and emissions on future sulfate-nitrate-ammonium aerosol levels in the United States, J. Geophys. Res., 114(D1), D01205, doi:10.1029/2008JD010701, 2009.

Qian, B., Corte-Real, J. and Xu, H.: Is the North Atlantic Oscillation the most important atmospheric pattern for precipitation in Europe?, J. Geophys. Res., 105(D9), 11901, doi:10.1029/2000JD900102, 2000.

Rattigan, O. V., Felton, H. D., Bae, M.-S., Schwab, J. J. and Demerjian, K. L.: Comparison of long-term $PM_{2.5}$ carbon measurements at an urban and rural location in New York, Atmos. Environ., 45(19), 3228–3236, doi:10.1016/j.atmosenv.2011.03.048, 2011.

Redmond, K. T. and Koch, R. W.: Surface Climate and Streamflow Variability in the Western United States and Their Relationship to Large-Scale Circulation Indices, Water Resour. Res., 27(9), 2381–2399, doi:10.1029/91WR00690, 1991.

Sauvage, B., Martin, R. V., van Donkelaar, A., Liu, X., Chance, K., Jaeglé, L., Palmer, P. I., Wu, S. and Fu, T.-M.: Remote sensed and in situ constraints on processes affecting tropical tropospheric ozone, Atmos. Chem. Phys., 7(3), 815–838, doi:10.5194/acp-7-815-2007, 2007.

Sheridan, S. C.: North American weather-type frequency and teleconnection indices, Int. J. Climatol., 23(1), 27–45, doi:10.1002/joc.863, 2003.

974 Singh, A. and Palazoglu, A.: Climatic variability and its influence on ozone and PM
975 pollution in 6 non-attainment regions in the United States, Atmos. Environ., 51,
976 212–224, doi:10.1016/j.atmosenv.2012.01.020, 2012.

977 Tai, A. P. K., Mickley, L. J., Jacob, D. J., Leibensperger, E. M., Zhang, L., Fisher, J. A.
978 and Pye, H. O. T.: Meteorological modes of variability for fine particulate matter
979 ($PM_{2.5}$) air quality in the United States: implications for $PM_{2.5}$ sensitivity to climate
980 change, Atmos. Chem. Phys., 12(6), 3131–3145,
981 doi:10.5194/acp-12-3131-2012, 2012a.

982 Tai, A. P. K., Mickley, L. J. and Jacob, D. J.: Correlations between fine particulate
983 matter ($PM_{2.5}$) and meteorological variables in the United States: Implications for
984 the sensitivity of $PM_{2.5}$ to climate change, Atmos. Environ., 44(32), 3976–3984,
985 doi:10.1016/j.atmosenv.2010.06.060, 2010.

986 Tai, A. P. K., Mickley, L. J. and Jacob, D. J.: Impact of 2000–2050 climate change on
987 fine particulate matter ($PM_{2.5}$) air quality inferred from a multi-model analysis of
988 meteorological modes, Atmos. Chem. Phys., 12(23), 11329–11337,
989 doi:10.5194/acp-12-11329-2012, 2012b.

990 Unger, N., Shindell, D. T., Koch, D. M., Amann, M., Cofala, J. and Streets, D. G.:
991 Influences of man-made emissions and climate changes on tropospheric ozone,
992 methane, and sulfate at 2030 from a broad range of possible futures, J. Geophys.
993 Res., 111(D12), D12313, doi:10.1029/2005JD006518, 2006.

994 van der Werf, G. R., Randerson, J. T., Giglio, L., Collatz, G. J., Kasibhatla, P. S. and
995 Arellano, A. F.: Interannual variability of global biomass burning emissions from
996 1997 to 2004, Atmos. Chem. Phys, 6, 3423-3441, doi:
997 10.5194/acpd-6-3175-2006, 2006.

998 van Donkelaar, A., Martin, R. V., Park, R. J.: Estimating ground-level $PM_{2.5}$ using
999 aerosol optical depth determined from satellite remote sensing, J. Geophys. Res.,
1000 111(D21), D21201, doi:10.1029/2005JD006996, 2006.

1001 van Donkelaar, A., Martin, R. V., Park, R. J., Heald, C. L., Fu, T. M., Liao, H. and
1002 Guenther, A.: Model evidence for a significant source of secondary organic
1003 aerosol from isoprene, Atmos. Environ., 41(6), 1267–1274,
1004 doi:10.1016/j.atmosenv.2006.09.051, 2007.

1005 van Donkelaar, A., Martin, R. V., Leaitch, W. R., Macdonald, A. M., Walker, T. W.,
1006 Streets, D. G., Zhang, Q., Dunlea, E. J., Jimenez, J. L., Dibb, J. E., Huey, L. G.,
1007 Weber, R. and Andreae, M. O.: Analysis of aircraft and satellite measurements
1008 from the Intercontinental Chemical Transport Experiment (INTEX-B) to quantify
1009 long-range transport of East Asian sulfur to Canada, Atmos. Chem. Phys., 8(11),
1010 2999–3014, doi:10.5194/acp-8-2999-2008, 2008.

1011 Vestreng, V., Myhre, G., Fagerli, H., Reis, S. and Tarrasón, L.: Twenty-five years of
1012 continuous sulphur dioxide emission reduction in Europe, Atmos. Chem. Phys.,
1013 7(13), 3663–3681, doi:10.5194/acp-7-3663-2007, 2007.

1014 Wallace, J. M. and Gutzler, D. S.: Teleconnections in the Geopotential Height Field
1015 during the Northern Hemisphere Winter, Mon. Weather Rev., 109(4), 784–812,
1016 doi:10.1175/1520-0493(1981)109<0784:TITGHF>2.0.CO;2, 1981.

1017 Wang H, Chen H and Liu J: Arctic Sea Ice Decline Intensified Haze Pollution in
1018 Eastern China, Atmospheric and Oceanic Science Letters, 8(1), 1–9,
1019 doi:10.3878/AOSL20140081, 2015.

1020 Wang, Y., Logan, J. A. and Jacob, D. J.: Global simulation of tropospheric O_3
1021 -NO_x-hydrocarbon chemistry: 2. Model evaluation and global ozone budget, J.
1022 Geophys. Res., 103(D9), 10727, doi:10.1029/98JD00157, 1998.

1023 Wesely, M. L.: Parameterization of surface resistances to gaseous dry deposition in
1024 regional-scale numerical models, Atmos. Environ., 23(6), 1293–1304,
1025 doi:10.1016/0004-6981(89)90153-4, 1989.

1026 Wheeler, M. C. and Hendon, H. H.: An all-season real-time multivariate MJO index:
1027 Development of an index for monitoring and prediction, Mon. Weather Rev.,
1028 132(8), 1917–1932,
1029 doi: 10.1175/1520-0493(2004)132<1917:AARMMI>2.0.CO;2,, 2004.

1030 Wise, E. K. and Comrie, A. C.: Meteorologically adjusted urban air quality trends in the
1031 Southwestern United States, Atmos. Environ., 39(16), 2969–2980,
1032 doi:10.1016/j.atmosenv.2005.01.024, 2005.

1033 Wu, S., Mickley, L. J., Jacob, D. J., Logan, J. A., Yantosca, R. M. and Rind, D.: Why
1034 are there large differences between models in global budgets of tropospheric
1035 ozone?, J. Geophys. Res., 112(D5), D05302, doi:10.1029/2006JD007801, 2007.

1036 Xiao, D., Li, Y., Fan, S., Zhang, R., Sun, J. and Wang, Y.: Plausible influence of
1037 Atlantic Ocean SST anomalies on winter haze in China, Theor. Appl. Climatol.,
1038 doi:10.1007/s00704-014-1297-6, 2014.

1039 Yang, Y., Liao, H. and Lou, S.: Decadal trend and interannual variation of outflow of
1040 aerosols from East Asia: Roles of variations in meteorological parameters and
1041 emissions, Atmos. Environ., 100, 141–153, doi:10.1016/j.atmosenv.2014.11.004,
1042 2015.

1043 Yienger, J. J. and Levy, H.: Empirical model of global soil-biogenic NO_x emissions, J.
1044 Geophys. Res., 100(D6), 11447, doi:10.1029/95JD00370, 1995.

1045 Zhang, G. J. and McFarlane, N. A.: Sensitivity of climate simulations to the
1046 parameterization of cumulus convection in the Canadian climate centre general
1047 circulation model, Atmosphere-Ocean, 33(3), 407–446,
1048 doi:10.1080/07055900.1995.9649539, 1995.

1049 Zhang, L., Jacob, D. J., Knipping, E. M., Kumar, N., Munger, J. W., Carouge, C. C.,
1050 van Donkelaar, A., Wang, Y. X. and Chen, D.: Nitrogen deposition to the United
1051 States: distribution, sources, and processes, Atmos. Chem. Phys., 12(10),
1052 4539–4554, doi:10.5194/acp-12-4539-2012, 2012.

1053 Zhang, L., Kok, J. F., Henze, D. K., Li, Q. and Zhao, C.: Improving simulations of fine
1054 dust surface concentrations over the western United States by optimizing the
1055 particle size distribution, Geophys. Res. Lett., 40(12), 3270–3275,
1056 doi:10.1002/grl.50591, 2013.

1057 Zhou, Z.-Q., Xie, S.-P., Zheng, X.-T., Liu, Q. and Wang, H.: Global Warming–Induced
1058 Changes in El Niño Teleconnections over the North Pacific and North America, J.
1059 Clim., 27(24), 9050–9064, doi:10.1175/JCLI-D-14-00254.1, 2014.

1060 Zhu, J., Liao, H. and Li, J.: Increases in aerosol concentrations over eastern China due
1061 to the decadal-scale weakening of the East Asian summer monsoon, Geophys.
1062 Res. Lett., 39(9), L09809, doi:10.1029/2012GL051428, 2012.

1063

1064

Table 1. The absolute (μg m^{-3}) and relative (%) differences in observed aerosol concentrations between the PNA+ and PNA– months (PNA+ minus PNA–). The observed concentrations are averaged over all the sites in the whole of U.S., in the western U.S., or in the eastern U.S.. See Fig 1 for locations of the sites. The measurements are from the EPA-AQS data. The ** and * indicate the differences that have passed the two-tail student-t test with 95% and 90% significance levels, respectively.

	Whole U.S.	Western U.S.	Eastern U.S
$PM_{2.5}$	1.0 (8.7%)**	1.3 (14.3%)**	0.8 (7.2%)**
SO_4^{2-}	0.01 (0.5%)	0.03 (3.2%)	0.1 (3.7%)
NO_3^-	0.3 (29.1%)**	0.2 (23.8%)**	0.4 (36.5%)**
NH_4^+	0.1 (11.9%)*	0.2 (31.6%)**	0.1 (10.5%)
OC	0.6 (13.5%)**	0.9 (17.7%)**	0.3 (8.0%)**
BC	0.2 (27.8%)**	0.2 (25.0%)**	0.1 (25.2%)**

Table 2. The absolute (μg m^{-3}) and relative (%) differences in simulated aerosol concentrations between the PNA+ and PNA– months (PNA+ minus PNA–). The simulated concentrations are averaged over the whole of U.S., the western U.S. (west of 100°W), or the eastern U.S. (east of 100°W). The concentrations are from the GEOS-Chem simulation for 1986–2006. The ** and * indicate the differences that have passed the two-tail student-t test with 95% and 90% significance levels, respectively.

	Whole U.S.	Western U.S.	Eastern U.S.
$PM_{2.5}$	0.6 (12.2%)**	0.3 (14.0%)**	0.9 (10.8%)**
SO_4^{2-}	0.2 (7.1%)	0.1 (13.5%) **	0.2 (4.0%)
NO_3^-	0.2 (30.3%) **	0.1 (28.5%) **	0.4 (33.5%)**
NH_4^+	0.2 (14.4%)**	0.1 (15.4%)**	0.2 (13.2%)**
OC	0.05 (6.5%)**	0.03 (8.6%)**	0.08 (5.9%)**
BC	0.03 (10.2%)**	0.01 (8.6%)**	0.05 (11.0%)**

Table 3. The composite analyses of horizontal mass fluxes (kg s^{-1}) of $PM_{2.5}$ for the selected box of (75–120°W, 28–49°N, from the surface to 250 hPa) in the PNA+ and PNA– months of 1986–2006. The positive values at the four boundaries indicate eastward or northward transport, and negative values indicate westward or southward transport. The positive (negative) value of net flux indicates the net gain (loss) of $PM_{2.5}$ in the selected box. All the fluxes are from the GEOS-Chem simulation.

	Boundaries and total	Mass Flux
PNA+	West	75.0
	East	233.9
	South	15.0
	North	–22.9
	Net flux	–120.9
PNA–	West	91.1
	East	247.4
	South	30.8
	North	8.8
	Net flux	–134.2
Diff. (PNA+ minus PNA–)	West	–16.1
	East	–13.5
	South	–15.8
	North	–31.7
	Net flux	13.3

Table 4. The pattern correlation coefficients between the composite differences in aerosol concentrations (Fig. 5c) and the corresponding composite differences in meteorological parameters (Fig. 7b). The * denotes the correlations that have passed the two-tail t-test with 95% confidence level.

	$PM_{2.5}$	SO_4^{2-}	NO_3^-	NH_4^+	OC	BC
T	–0.13	0.26*	–0.59*	–0.22*	0.07	–0.16
PR	–0.44*	–0.38*	0.04	–0.42*	–0.63*	–0.50*
RH	–0.08	–0.05	–0.02	0.12	–0.32*	–0.36*
WS	–0.27*	–0.1	–0.22*	–0.27*	–0.28*	–0.24*
PBLH	–0.61*	–0.43*	–0.32*	–0.61*	–0.60*	–0.55*

Figure Captions

Fig. 1. The locations of EPA-AQS sites with measurements that meet the criteria described in Sect. 2.1 in the text. $PM_{2.5}$ measurements are available for years of 1999–2013 (sites are marked by black dots) and speciated aerosol (SO_4^{2-}, NO_3^-, NH_4^+, BC, and OC) concentrations are available over years of 2000–2013 (sites are marked by red diamonds). The grey solid line defines the western United States (west of 100°W) and eastern United States (east of 100°W).

Fig. 2. (a) PNAI for years of 1986–2013 calculated using the NCEP-2 data (NCEP2-PNAI), with the PNA+ and PNA– months during 1999–2013 indicated. (b) PNAI for years of 1986–2013 calculated using the NCEP-2 data, with the PNA+ and PNA– months during 2000–2013 indicated. (c) PNAI for years of 1986–2006 calculated using the GEOS-4 data (GEOS4-PNAI), with the PNA+ and PNA– months over 1986–2006 indicated. Red circles are PNA+ months and blue circles PNA– months. The PNA+ (PNA–) months are defined as the 25% of winter months examined, which have the highest positive (negative) PNA index values.

Fig. 3. The absolute ($\mu g\ m^{-3}$, left column) and relative differences (%, right column) in observed monthly mean aerosol concentrations between PNA+ and PNA– months (PNA+ minus PNA–). See Fig. 2c for the definitions of PNA+ and PNA– months. The measurements of $PM_{2.5}$ were carried out over 1999–2013, in which there were 18 PNA+ months and 18 PNA– months as shown in Fig. 2a. The measurements of speciated aerosols were taken during 2000–2013, in which there were 17 PNA+ and 17 PNA– months (Fig. 2b). The seasonal cycle and trend in observed aerosol concentrations were removed as described in Sect. 2.1. The sites with black dots were the differences that passed the two-tail t-test with 90% confidence level.

Fig. 4. (a) Simulated surface-layer concentrations ($\mu g\ m^{-3}$) of $PM_{2.5}$ (the sum of SO_4^{2-}, NO_3^-, NH_4^+, BC, and OC) and each aerosol species averaged over NDJFM of 1999–2006. (b) Scatter plots of the simulated concentrations ($\mu g\ m^{-3}$, vertical axis) versus the EPA-AQS observations ($\mu g\ m^{-3}$, horizontal axis). Also shown are the y=x line (black dash line), linear fit for whole U.S. (black line), linear fit for western U.S. (blue line), and linear fit for eastern U.S. (red line). The blue and red dots represent sites in the western and eastern U.S., respectively. (c) Comparisons of the deviation from the mean (DM) of observed concentration (black line) with that of simulated concentration (red line) in each winter month for each aerosol species, left axis. Also shown in the panel for OC (BC) the monthly variation in DM of biomass burning emission of OC (BC), blue line, right axis.

Fig. 5. (a) Simulated concentrations ($\mu g\ m^{-3}$) of $PM_{2.5}$ and each aerosols species averaged over the PNA– months of 1986–2006. (b) The absolute differences ($\mu g\ m^{-3}$) in simulated aerosol concentrations between PNA+ and PNA– months (PNA+ minus PNA–). (c) The relative differences (%) in simulated aerosol concentrations between PNA+ and PNA– months. The white spaces in (C)

indicate the areas that did not pass the two-tail student-t test with 90% significance level. The seasonal cycles of simulated aerosol concentrations were removed. See Fig. 2c for the definitions of PNA+ and PNA– months.

Fig. 6. (a) Horizontal winds at 700 hPa averaged over the winter months of NDJFM of 1986–2006, and (b) the corresponding differences between the PNA+ and PNA– months. Datasets are from the assimilated GEOS-4 meteorological fields. Also shown in (b) is the domain of (75–120°W, 28–49°N) for which transboundary mass fluxes of $PM_{2.5}$ are calculated. See Fig. 2c for the definitions of PNA+ and PNA– months.

Fig. 7. (a) The absolute and (b) relative differences in meteorological parameters between PNA+ and PNA– months. Datasets are from the assimilated GEOS-4 meteorological fields. The white spaces in indicate the areas that did not pass the two-tail student-t test with 90% significance level. The seasonal cycles of meteorological variables were removed, similar to the treatment for observations in Fig. 3. See Fig. 2c for the definitions of PNA+ and PNA– months.

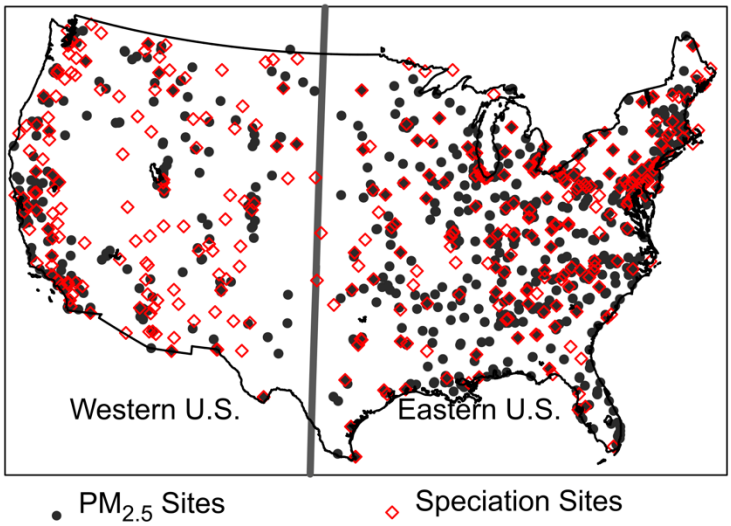

Fig. 1. The locations of EPA-AQS sites with measurements that meet the criteria described in Sect. 2.1 in the text. $PM_{2.5}$ measurements are available for years of 1999–2013 (sites are marked by black dots) and speciated aerosol (SO_4^{2-}, NO_3^-, NH_4^+, BC, and OC) concentrations are available over years of 2000–2013 (sites are marked by red diamonds). The grey solid line defines the western United States (west of 100°W) and eastern United States (east of 100°W).

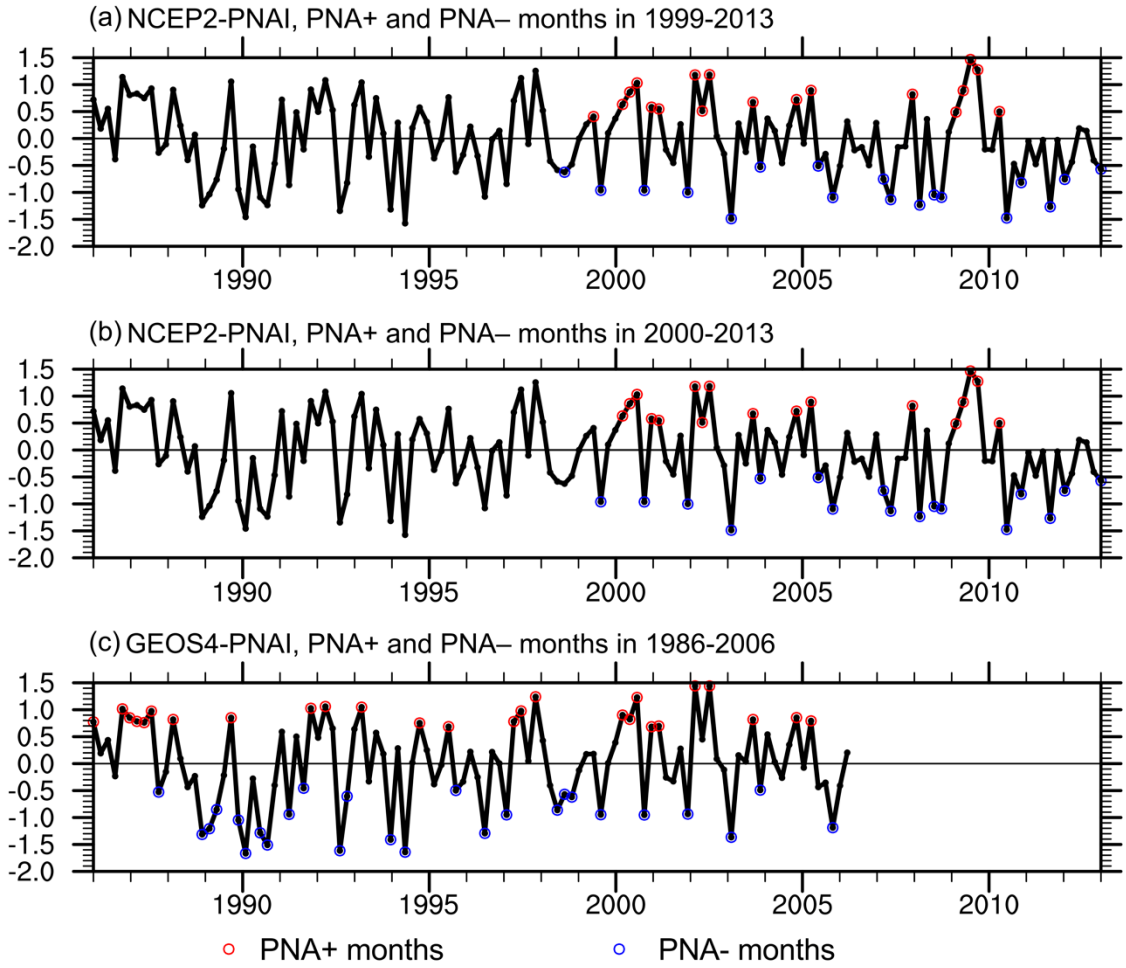

Fig. 2. (a) PNAI for years of 1986–2013 calculated using the NCEP-2 data (NCEP2-PNAI), with the PNA+ and PNA– months during 1999–2013 indicated. (b) PNAI for years of 1986–2013 calculated using the NCEP-2 data, with the PNA+ and PNA– months during 2000–2013 indicated. (c) PNAI for years of 1986–2006 calculated using the GEOS-4 data (GEOS4-PNAI), with the PNA+ and PNA– months over 1986–2006 indicated. Red circles are PNA+ months and blue circles PNA– months. The PNA+ (PNA–) months are defined as the 25% of winter months examined, which have the highest positive (negative) PNA index values.

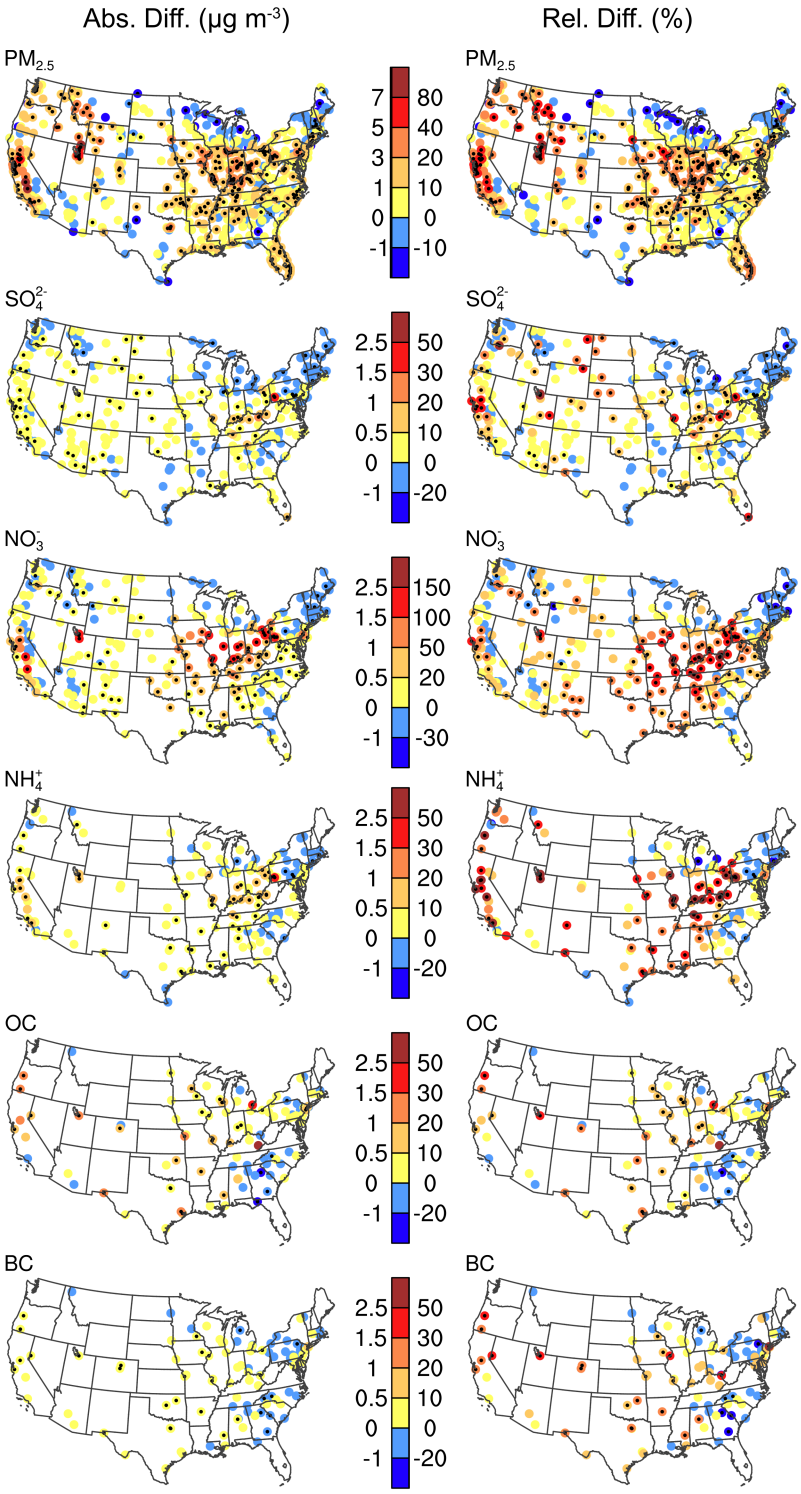

Fig. 3. The absolute (μg m^{-3}, left column) and relative differences (%, right column) in observed monthly mean aerosol concentrations between PNA+ and PNA– months (PNA+ minus PNA–). See Fig. 2c for the definitions of PNA+ and PNA– months. The measurements of $PM_{2.5}$ were carried out over 1999–2013, in which there were 18 PNA+ months and 18 PNA– months as shown in Fig. 2a. The measurements of speciated aerosols were taken during 2000–2013, in which there were 17 PNA+ and 17 PNA– months (Fig. 2b). The seasonal cycle and trend in observed aerosol concentrations were removed as described in Sect. 2.1. The sites with black dots were the differences that passed the two-tail t-test with 90% confidence level.

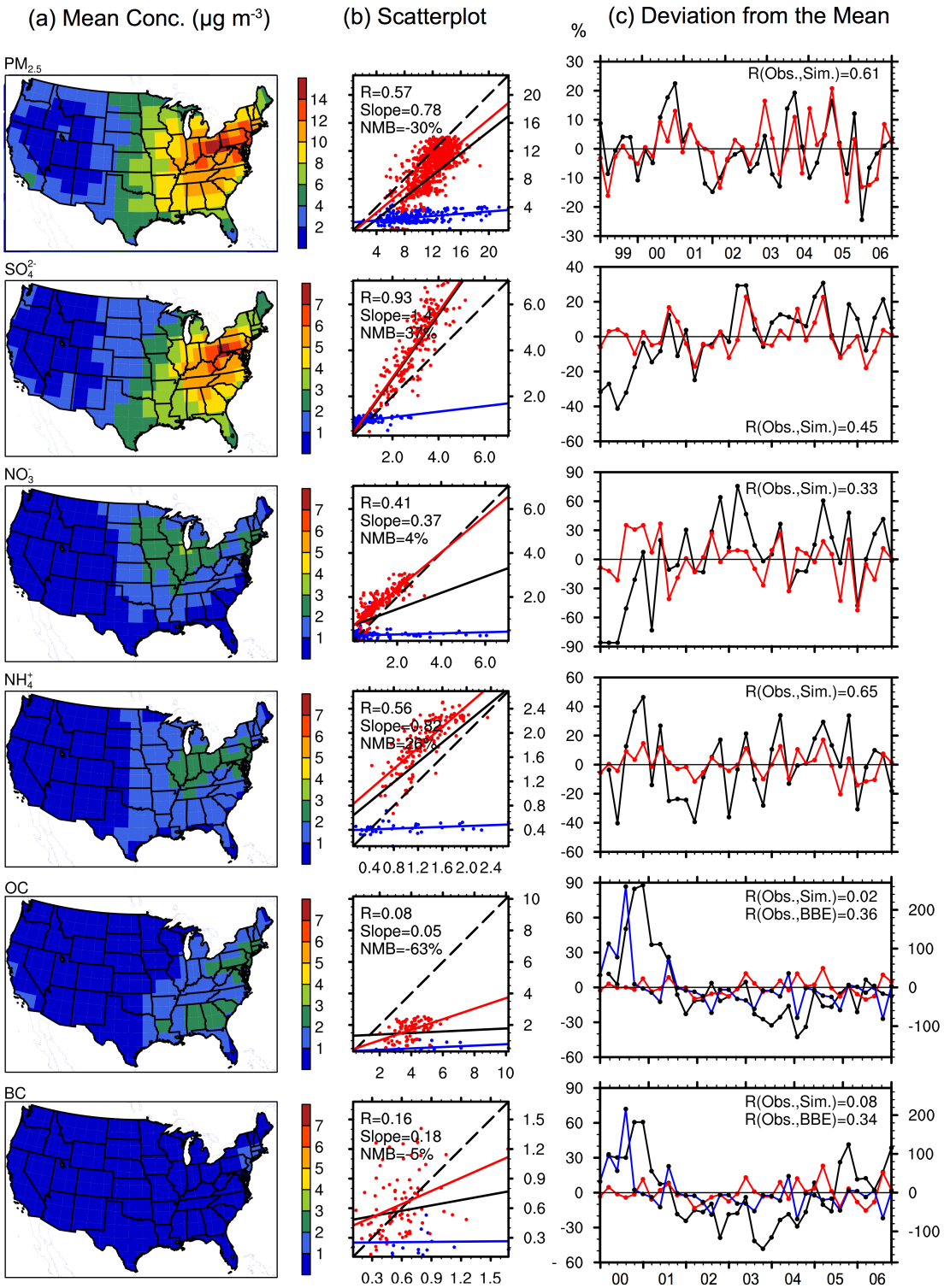

Fig. 4. (a) Simulated surface-layer concentrations (μg m^{-3}) of $PM_{2.5}$ (the sum of SO_4^{2-}, NO_3^-, NH_4^+, BC, and OC) and each aerosol species averaged over NDJFM of 1999–2006. (b) Scatter plots of the simulated concentrations (μg m^{-3}, vertical axis) versus the EPA-AQS observations (μg m^{-3}, horizontal axis). Also shown are the y=x line (black dash line), linear fit for whole U.S. (black line), linear fit for western U.S. (blue line), and linear fit for eastern U.S. (red line). The blue and red dots represent sites in the western and eastern U.S., respectively. (c) Comparisons of the deviation from the mean (DM) of observed concentration (black line) with that of simulated concentration (red line) in each winter month for each aerosol species, left axis. Also shown in the

1198 panel for OC (BC) the monthly variation in DM of biomass burning emission of OC
1199 (BC), blue line, right axis.

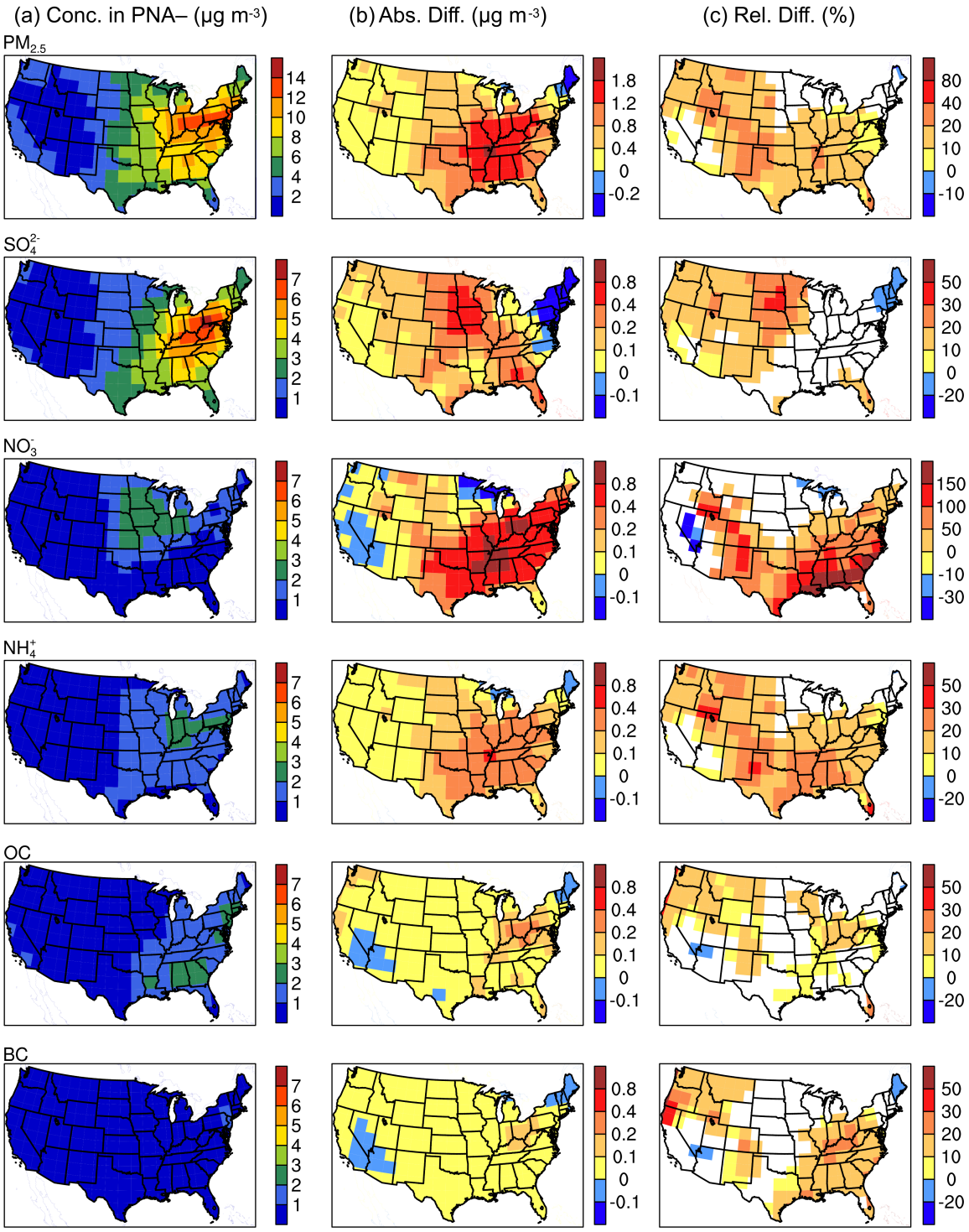

Fig. 5. (a) Simulated concentrations (μg m^{-3}) of $PM_{2.5}$ and each aerosols species averaged over the PNA– months of 1986–2006. (b) The absolute differences (μg m^{-3}) in simulated aerosol concentrations between PNA+ and PNA– months (PNA+ minus PNA–). (c) The relative differences (%) in simulated aerosol concentrations between PNA+ and PNA– months. The white spaces in (C) indicate the areas that did not pass the two-tail student-t test with 90% significance level. The seasonal cycles of simulated aerosol concentrations were removed, similar to the treatment for observations in Fig. 3. See Fig. 2c for the definitions of PNA+ and PNA– months.

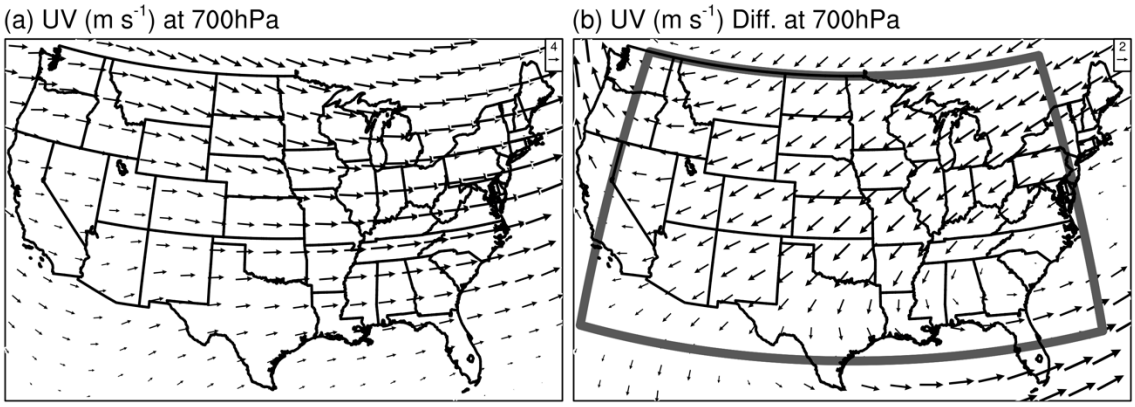

Fig. 6. (a) Horizontal winds at 700 hPa averaged over the winter months of NDJFM of 1986–2006, and (b) the corresponding differences between the PNA+ and PNA– months. Datasets are from the assimilated GEOS-4 meteorological fields. Also shown in (b) is the domain of (75–120°W, 28–49°N) for which transboundary mass fluxes of $PM_{2.5}$ are calculated. See Fig. 2c for the definitions of PNA+ and PNA– months.

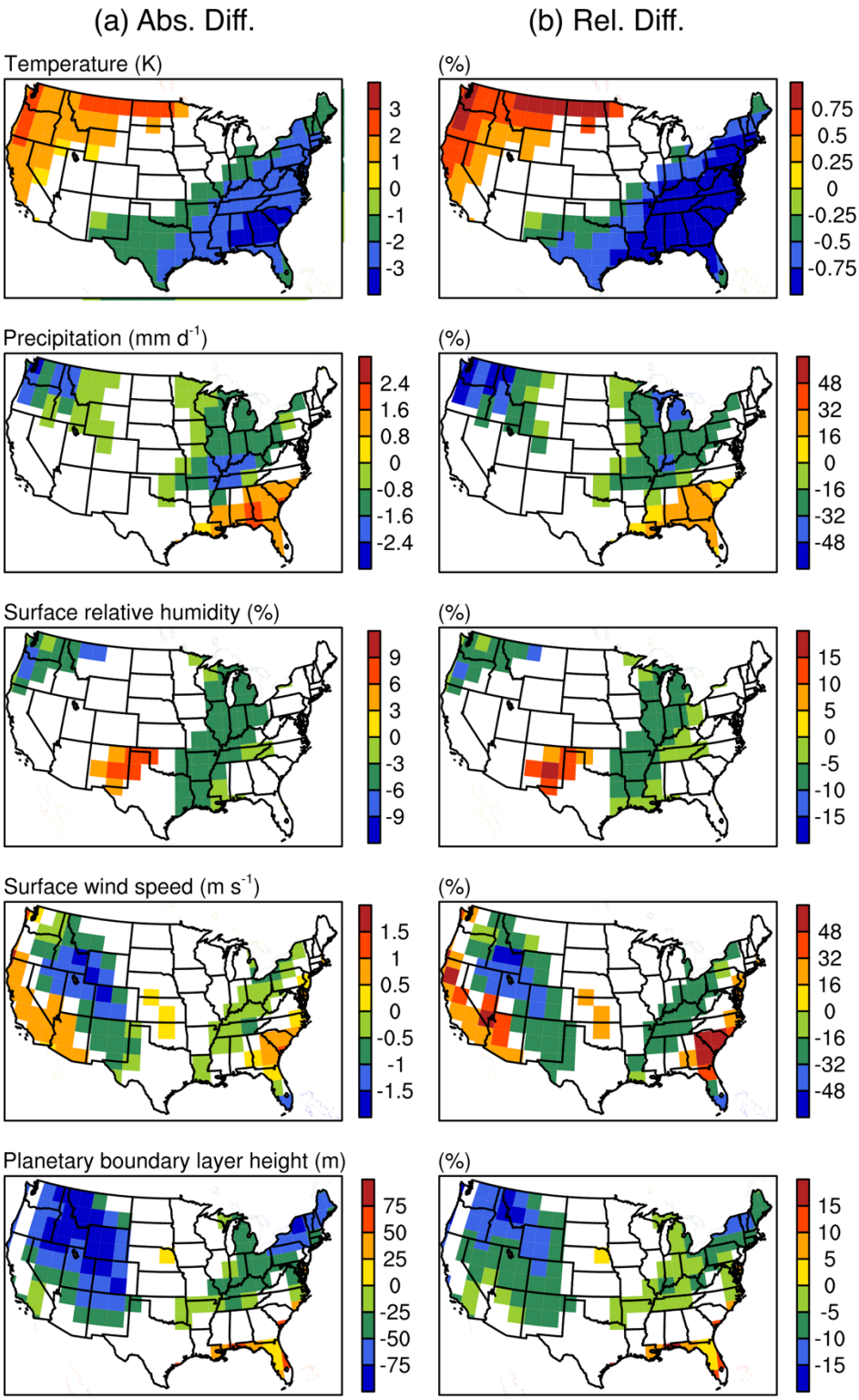

Fig. 7. (a) The absolute and (b) relative differences in meteorological parameters between PNA+ and PNA– months. Datasets are from the assimilated GEOS-4 meteorological fields. The white spaces in indicate the areas that did not pass the two-tail student-t test with 90% significance level. The seasonal cycles of meteorological variables were removed, similar to the treatment for observations in Fig. 3. See Fig. 2c for the definitions of PNA+ and PNA– months.

1223